International Journal of SPACE STRUCTURES

Article

Equivalent static loads for double-layered domes supported by multistorey buckling-restrained braced frames

International Journal of Space Structures
1–34

DOI: 10.1177/09560599221097834
journals.sagepub.com/home/sps
SAGE

Deepshikha Nair[1], Yuki Terazawa[1] and Toru Takeuchi[1]

Abstract

Curved gridshells are excited not only in the horizontal direction but also experience large anti-symmetric vertical accelerations when subjected to horizontal earthquake ground motions. In addition to the coupled response, gridshells exhibit closely spaced modes and substructure-roof interaction. Nevertheless, previous studies have proposed elastic horizontal and vertical equivalent static seismic forces considering these complex dynamic response characteristics. These are determined from the input horizontal acceleration at the substructure's roof level, an assumed acceleration distribution, nodal roof masses and amplification factors derived from the dynamic characteristics of the dome and substructure. To extend this methodology to nonlinear substructures with displacement-dependent damping devices, this paper investigates the applicability of ductility reduction factors (or R_μ factors) to estimate the inelastic response spectra and an alternative equivalent linearisation approach to compute the peak horizontal acceleration of multistorey substructures with buckling-restrained braces. This is achieved by modelling the curved roof as a rigid mass for the substructure model, and using its idealised base shear-roof displacement relationship obtained from modal pushover analyses. The peak horizontal acceleration of the substructure is then used to obtain the equivalent static loads of the curved roof using amplification factors, and the accuracies are verified against the results from nonlinear response history analyses. It was confirmed that the R_μ factors combined with the roof amplification factors provide a simple way to estimate the peak roof response with sufficient accuracy for preliminary design of domes with multistorey substructures having low post-yield stiffness.

Keywords

Double-layered domes, seismic response, hysteretic dampers, elastoplastic model, multistorey substructures, R-factors, equivalent static loads, buckling-restrained braced frames

Introduction

Equivalent static lateral force method often forms the precedent for seismic design of (regular) nonlinear multistorey buildings as prescribed by most design codes like the ASCE-7-16,[1] NZS1170.5,[2] Eurocode 8[3] and the Building Standard Law of Japan.[4] For example, the ASCE-7-16 provides response reduction factors (*R*-factors[1]), to estimate the design base shear and the horizontal storey forces based on the type of buildings. However, gridshells are often treated as irregular or special structures owing to the complex roof-substructure interaction and closely-spaced multiple participating modes[5,6] and therefore require advanced analyses. Modal response-spectrum analyses (RSA) is a relatively simple and efficient method often used to compute the peak response of elastic gridshell domes and are recommended in code specifications.[6–8] The method estimates the peak response of each

[1]Tokyo Institute of Technology, Meguro-ku, Japan

Corresponding author:
Deepshikha Nair, Department of Architecture and Building Engineering, Tokyo Institute of Technology, 2-12-1-M1-29 Ookayama, Meguro-ku, Tokyo 152-8550, Japan.
Email: nair.d.aa@m.titech.ac.jp

participating mode using the spectral acceleration of the elastic design spectrum and combines the modal responses as per the appropriate combination rule. In the context of gridshell structures, its application is limited to elastic structures as it can not be extended to domes with nonlinear substructures as there are no prescribed scaling or response reduction factors for higher modes nor is it evident how multistorey substructures response estimated using the standard reduction factors can be applied for roof structures.[5,6]

Metal gridshells supported by substructures in regions of severe seismic hazard need to be designed to withstand the high seismic demand. The seismic response of roofs with simple symmetric lattice geometries like the arch, dome, and cylinder have been extensively studied by varying the parameters like the span (30–150 m), half-subtended angle (20°–40°), out-of-plane stiffness, rise-to-span ratios, and substructure stiffness.[6,7,9–13] It was found that increasing the out-of-plane bending stiffness of the members prevented failure due to buckling that is common in single-layer roofs. The number of participating modes are also reduced and the response can be simply estimated as a function of four dominant modes – three anti-symmetric modes ('O1', 'O2' and 'O2.5') and an in-plane mode 'I'.[5,7,14] For roofs with supporting substructures, the seismic input amplifies up the substructure height and the substructure roof's horizontal acceleration acts as the input for the gridshell roof. The geometry and dynamic characteristics of gridshell lead to its coupled horizontal and anti-symmetric vertical roof response. In an attempt to develop equivalent static loads, these elastic substructure-roof interactions have been investigated[13,15] and quantified as horizontal and vertical amplification factors that are functions of the substructure to roof's period ratios. The vertical response was found to amplify by up to three times the input horizontal seismic input at the substructure roof level.[7] Further increasing the height of the substructure leads to increased participation from the higher substructure modes and the interaction between the higher substructure modes (in linear range) and dominant roof modes have also been quantified as higher mode amplification factors.[16]

Gridshell roofs are often employed in school gymnasiums or community centres which are expected to be functional as shelters even after a big earthquake in countries of high seismic hazard like Japan. Consequently, it becomes important to design such structures with seismic response control strategies. One efficient solution to limit the roof seismic demand by decreasing the peak substructure response is to add damping devices such as the hysteretic buckling-restrained braces (BRB) to the substructure frames[17] and the response estimation of such systems have also been studied[8,13,18,19] using Kasai's equivalent linearisation method.[20,21] This lowered demand enables the engineers to design the roofs such that they remain elastic and the reduced roof acceleration also ensures the seismic performance of acceleration sensitive non-structural components such as ceilings and lighting equipment. Practical applications of employing passive-control devices include the Toyota stadium,[22] Shimokita dome[23] and other seismic-retrofit projects of high-school gymnasiums.[24,25] While there exists well-established response-reduction factors for design and estimation of the inelastic design spectra of conventional BRB frames,[26,27] their application to substructures of curved gridshell roofs has not yet been explored. Therefore, as neither reliable static load procedures nor realistic R-factors are available for such structural systems, the time- and data-intensive nonlinear response history analysis (NLRHA) is often the only design route. With an aim to improve the preliminary design of such double-layered domes, this paper investigates the applicability of the ductility-based reduction factors (labelled as the 'R-factor approach') to estimate the peak substructure response using RSA which is used to propose equivalent static forces of the dome. The response of simpler single-storey substructures are first studied, and the response estimation methods are compared with the equivalent linearisation approach. The higher mode effects of multistorey substructures are then investigated using higher mode amplification factors for two-storey and six-storey analysis models and the results are verified using nonlinear response history analyses.

Seismic response characteristics of double-layered domes

Past studies on the seismic response of gridshell domes[7,8,13,14] have revealed that in addition to horizontal accelerations, double-layer domed gridshell roofs with some rise are excited not only in the horizontal direction but also experience large anti-symmetric vertical accelerations when subjected to horizontal earthquake ground motions (Figure 1(a)). In the case of relatively thin lattice domes, a large number of vibration modes with similar periods significantly participate in the response.[14] Nevertheless, it has been observed that when the out-of-plane stiffness of the roof is large (typical of double-layered domes[5]), the response characteristics are predominated by four prominent modes which are denoted as O1, O2, O2.5, and I shown in Figure 1(b)[7,13,16] where O1 is the fundamental mode and has an asymmetric modeshape with one crest and one trough (Figure 1(b)). The O2 mode is the next higher mode with two crests and two troughs with high amplitude in the centre wave, followed by the O2.5 mode that is similar to the O2 mode but has lower amplitudes. The fourth mode is the in-plane mode I, which has the shortest period as the in-plane stiffness of double-layered domes is relatively high. Equivalent lateral forces have also been proposed for medium-span domes with single-storey substructures

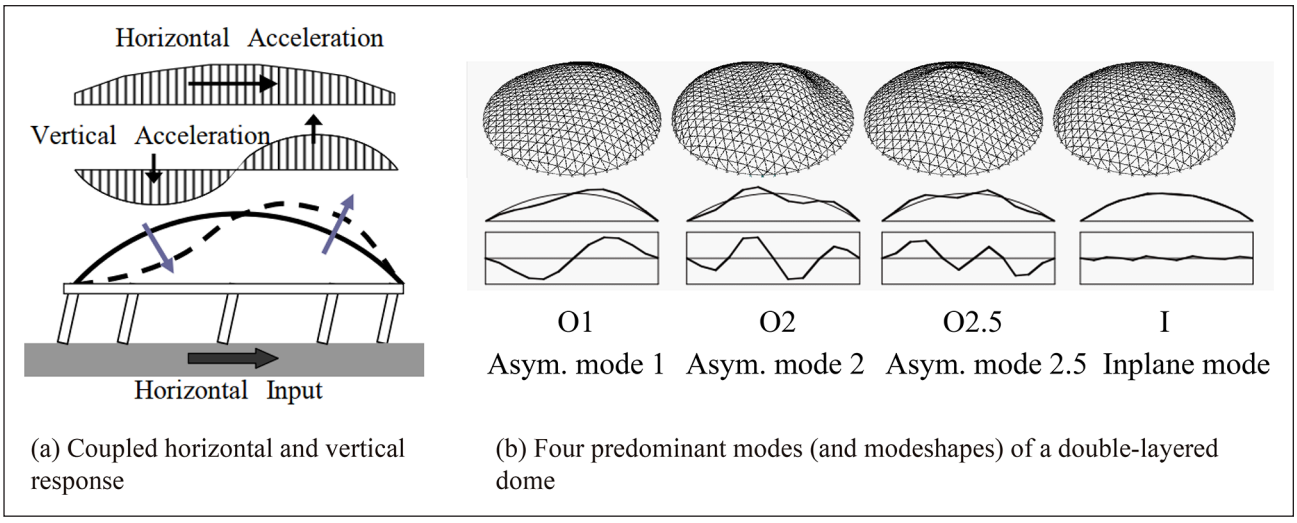

(a) Coupled horizontal and vertical response

(b) Four predominant modes (and modeshapes) of a double-layered dome

Figure 1. Seismic response characteristics of domes with substructures under horizontal seismic loading[7]: (a) coupled horizontal and vertical response and (b) four predominant modes (and modeshapes) of a double-layered dome.

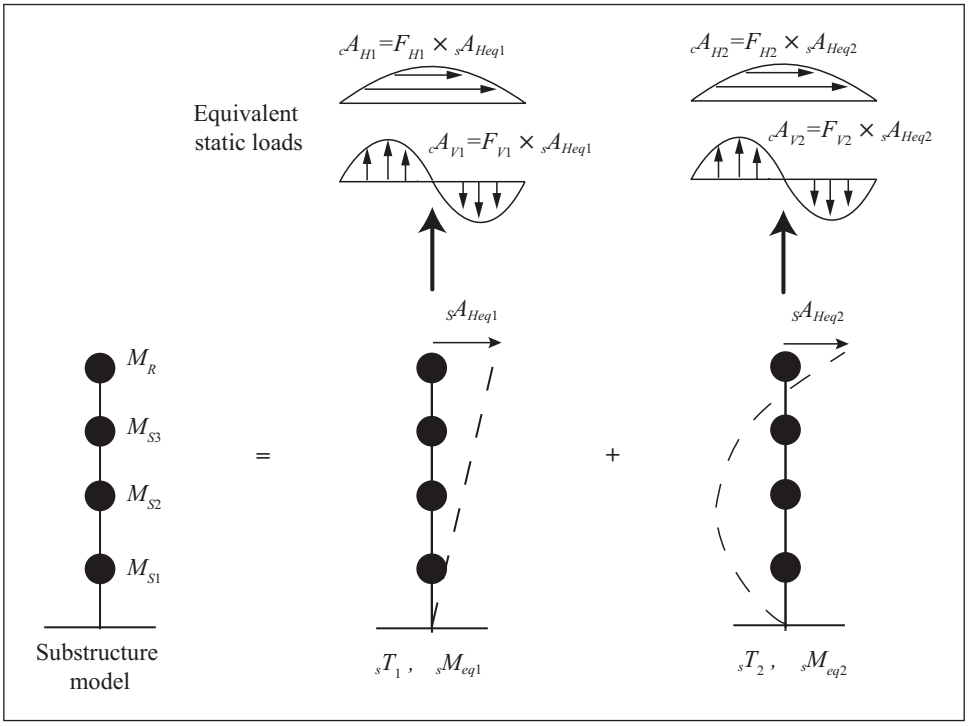

Figure 2. Equivalent static load procedure.[16]

using amplification factors (that quantify the roof-substructure interaction considering the four predominant roof modes).[7] To extend this method to multistorey substructures, horizontal and vertical amplification factors were proposed to estimate the roof response generated by higher multistorey substructure modes in interaction with the four roof modes.[16] Finally, a generalised equivalent static design procedure was developed (Figure 2) for domes with multistorey substructures and validated against RSA, comparing against both the nodal displacements and member forces.[15,16]

Peak substructure response

This section introduces the equivalent static load procedure and discusses two R-factor approaches and an

equivalent linearisation approach to estimate the peak substructure acceleration of a yielding substructure.

The peak substructure roof acceleration (A_{Heq}) is the seismic input for the dome and is the first step in the proposed equivalent static load procedure for linear double-layered domes with elastic substructures.[15,16] The substructure is modelled as a simple lumped-mass model as shown in Figure 2 with the roof modelled as a rigid mass (M_R) and the peak substructure acceleration is computed using response-spectrum analysis. The substructure acceleration for each participating mode is then multiplied by corresponding horizontal and vertical amplification factors to obtain the peak acceleration distributions of the dome using an assumed mode shape (usually the dominant mode O1).[7,16] The amplification factors quantify the roof-substructure interaction defined by the substructure to roof period and mass ratios.[7,13,16] These roof horizontal and vertical accelerations (Figure 2) are then multiplied by the nodal masses to obtain the equivalent inertial static forces.

Inelastic accelerations: RSA and R-factor

The total force reduction factor (or the response modification factor R) for idealised bilinear systems is derived as follows (Uang[28]) in equation (1) and Figure 3(a), where R_μ is the ductility reduction factor and Ω is the structural overstrength factor. R_μ accounts for the reduction in the elastic design force because of the energy dissipation capacity and the reserve strength that exists between the actual structural yield level and the first yield level is defined as Ω.[28] R_μ is therefore defined as the ratio of the elastic strength demand to the inelastic strength demand (equation (1)[28]) and is used to derive the inelastic seismic acceleration spectrum.

$$R = R_\mu \Omega \quad ; \quad R_\mu = \frac{F_y(\mu = 1)}{F_y(\mu = \mu_i)} \tag{1}$$

Newmark-Hall methodology. The Veletsos-Newmark-Hall methodology[30] (labelled and referred to as the 'Newmark' method hereon) is one of the earliest and commonly used methods to derive the inelastic seismic design spectra (Figure 3(b)), where the 5% damped spectrum for the elastoplastic system is obtained by drawing a curve similar to that of the elastic system but displaced downward by the reduction factor. The reduction factor proposed depends on the position of the period on the spectrum.

- For constant-acceleration region of the spectrum where the equal energy rule applies,[30] where the area under the load-deformation diagram up to the maximum deformation is the same as that of an elasto-perfectly plastic system:

$$R_\mu = \sqrt{2\mu - 1} \tag{2}$$

- For constant-velocity region of the spectrum where the equal displacement rule applies[30]:

$$R_\mu = \mu \tag{3}$$

Nassar and Krawinkler. To estimate the inelastic strength demands, strength reduction factors R_μ were derived as a function of the target ductility ratio μ and the period T, using a least square fit regression analysis for a single degree of freedom system with post-yield stiffness ratios (p) of 0%, 2%, and 10% subjected to 39,000 time history analyses for $T = 0.1$–4.0 s, $\mu = 1$–8 for a damping of 5%[31] given in equation (4) (labelled and referred to as the 'N&K' method hereon)

$$R_\mu = \left[c(\mu - 1) + 1\right]^{1/c}; \quad c = \frac{T^a}{T^a + 1} + \frac{b}{T} \tag{4}$$

where $a = 1$ for $p <= 2\%$, $a = 0.8$ for p = 10% and $b = 0.42, 0.37$ and 0.29 for p = 0%, 2%, and 10% respectively.

Lee and Han. Lee et al.[32] further studied the reduction factors for different hysteretic models and proposed R_μ as a function of the period and ductility using a two-stage regression analysis. The equations for elasto-perfectly plastic models are given in equations (5) and (6).

$$R_\mu = A_0\{1 - \exp(-B_0 \times T)\} \tag{5}$$

$$A_0 = 0.99 \times \mu + 0.15; \quad B_0 = 23.69 \times \mu^{-0.83} \tag{6}$$

For comparison, the reduction factors obtained from the three methods are plotted below considering a fundamental period in the short-period range as 0.4 s (period of the benchmark single-storey model discussed later) and elastoplastic behaviour.

While these ductility reduction factors were proposed to develop the inelastic response spectra to estimate the design base shear for elastoplastic models, in this study, these ductility reduction factors are used to estimate the approximate peak spectral acceleration of the substructure as a function of the obtained period and the target roof displacement ductility. The acceleration reduction ratio R_a is defined as the ratio of the peak inelastic acceleration to the peak elastic acceleration which can be computed using the inverse of the ductility reduction ratio[30] as shown in equation (7). For this

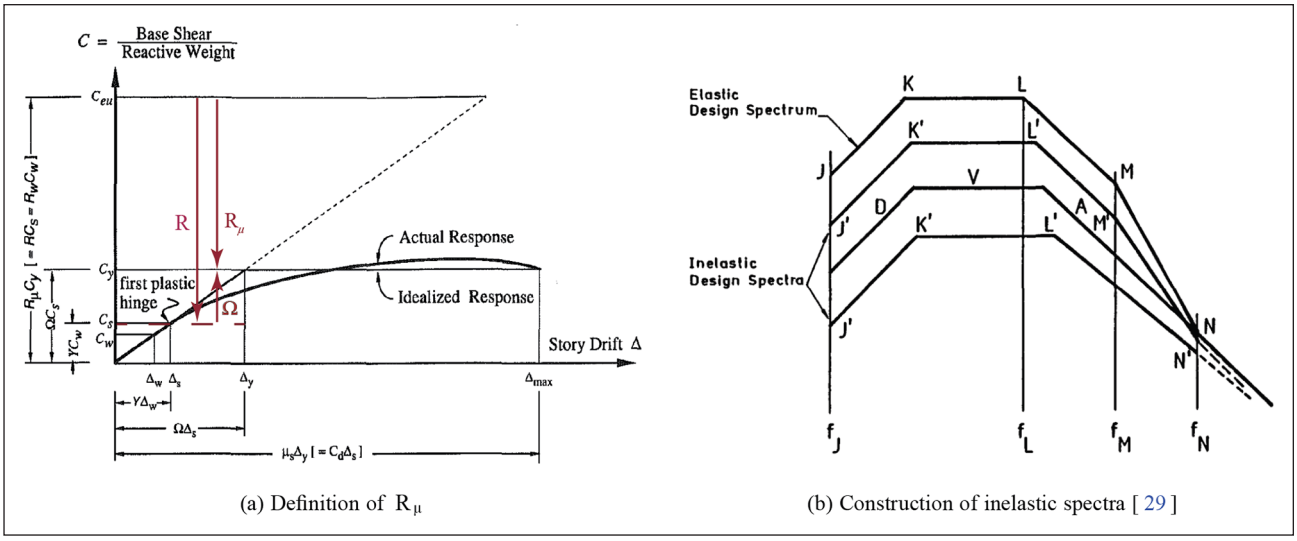

(a) Definition of R_μ (b) Construction of inelastic spectra [29]

Figure 3. (a) Idealisation of structural response and *R* factors, Picture taken from Uang.[28] (b) Construction of design spectra, Picture taken from Riddell et al.[29]

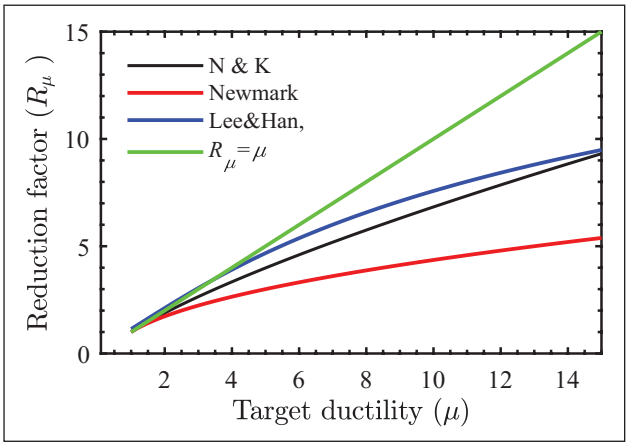

Figure 4. T = 0.4 s, reduction factor as a function of target ductility.

study, from hereon, the two most conservative methods – Newmark and N&K methods (Figure 4) are considered and discussed for the estimation of peak substructure acceleration using the R-factor approach.

$$R_a = \frac{A_{eq1}}{A_1}; \quad R_a = \frac{1}{R_\mu} \tag{7}$$

Inelastic accelerations: RSA and equivalent linearisation

An alternative simplified theory for estimation of the peak inelastic response of any bilinear system is the equivalent linearisation method proposed by Kasai and Ito.[20,21] It uses mathematical expressions as a function of the dynamic properties of the system to consider the effect of period shift as well as the effect of damping by evaluating the dissipated energy. The multistorey building is idealised as an SDOF (single-degree of freedom) model and the target ductility is iterated to obtain a more accurate ductility value which is a function of the achieved damping and the secant stiffness ratio which in turn is a function of the ductility. The proposed reduction in displacement R_d and acceleration (or force) R_a depends on the stiffness of the frame, braces, and the energy dissipation devices.

The equivalent stiffness (K_{eq}) and equivalent damping ratio (h_{eq}) of the system are obtained using the equivalent linearisation procedure. For each of the participating modes (where i = mode number), a starting value of ductility ratio (target ductility) μ_{ti} is assumed and h_{eqi} and the equivalent stiffness ratio K_{eqi}/K_{1i} are iterated using equations (8)–(11) until μ_i converges, where K_{1i} is the initial stiffness, D_h is the reduction factor to adjust the damping ratio from the base damping ratio h_{oi} (5% in this study) for periods less than 2 s, and the subscript (j) is the jth step of the iteration.[18,20] The equivalent (secant) period T_{eqi} is then computed using equation (12).[20]

$$K_{eqi}/K_{1i} = 1/\mu_i + (1-1/\mu_i)K_{2i}/K_{1i} \tag{8}$$

$$h_{eqi} = h_{oi} + \frac{2(K_{1i}/K_{2i})}{\pi\mu_i}\ln\frac{K_{1i}/K_{2i}+\mu_i-1}{(K_{1i}/K_{2i})\mu_i^{K_{2i}/K_{1i}}} \tag{9}$$

$$D_{hi} = \sqrt{(1+25h_{oi})/(1+25h_{eqi})} \tag{10}$$

$$\mu_{i(j)} = \mu_{ti(1)} D_{hi(j-1)} / \sqrt{K_{eqi(j-1)} / K_{1i}} \quad (11)$$

$$T_{eqi} = T_i \sqrt{K_{1i} / K_{eqi}} \quad (12)$$

For each of the participating modes, the reduction in displacement R_d and acceleration R_a can then be computed as a function of the periods T_{eqi} and T_i using equations (13)–(16)[20] depending on the regions of the spectrum the periods lie. This method is labelled and referred to as the 'Kasai' method hereon.

1. For T_i and T_{eqi} in the constant acceleration region:

$$R_{di} = D_{hi} \frac{T_{eqi}}{T_i} \left(\frac{T_{eqi} + T_i}{2T_i}\right) \quad (13)$$

2. For T_i in the constant acceleration region and T_{eqi} in the constant velocity region, where T_c is the corner period (in this study, $T_c = 0.52$ s as described later in Figure 7):

$$R_{di} = D_{hi} \frac{T_{eqi}}{T_i} \left[\frac{T_c}{T_i} - \frac{(T_c / T_i - 1)^2}{2(T_{eqi} / T_i - 1)}\right] \quad (14)$$

3. For T_i and T_{eqi} in the constant velocity region:

$$R_{di} = D_{hi} \frac{T_{eqi}}{T_i} \quad (15)$$

The reduction in acceleration may then be computed using equation (16).[20,21] For comparison of response with the other methods based on the R-factor approach, $R_{\mu i}$ from this method may then be defined as the inverse of the reduction in acceleration as given in equation (16).

$$R_{ai} = R_{di} \left(\frac{T_i}{T_{eqi}}\right)^2; \quad R_{\mu i} = \frac{1}{R_{ai}} \quad (16)$$

Analysis models: Single-storey substructures

First, the peak substructure response of simple single-storey analysis models are discussed in this section to compare the response from each of the response estimation methods.

Design acceleration spectrum

A site with high seismic hazard from the southern California region was chosen to develop a 5% damped DBE (design basis earthquake) acceleration spectrum (Figure 7) using the ASCE 7-16 procedure[1]) with $S_{DS} = 1.4g$ (short period spectral acceleration), $S_{D1} = 0.73g$ (spectral response acceleration at a period of 1 s), and $T_L = 8s$ (long-period transition period obtained from Figures 22 to 14 of ASCE 7-16[1]).

BRBF substructure model

The 60 m spanned substructure has one storey 5 m high and the roof dead load was assumed to be 2 kPa (considering a structural weight of about 1 kg/m^2 for every metre of span,[33] a 15% allowance for the connections, and 1.3 kPa nonstructural dead load). It was assumed that all the lateral forces are resisted by the buckling-restrained braces (BRBs[34]) placed along the perimeter in a diagonal configuration, and so in the 3-d ETABS[35] analysis substructure model shown in Figure 5(a), all the beams and columns were modelled using elastic beam and column elements with the section sizes listed in Table 1. The roof is modelled as a rigid mass in the substructure model. The BRBs for the substructure (Figure 5) were designed for the vertically distributed forces obtained as per ASCE 7-16,[1] where h_x is the height from base to level x and k is taken as 2 (equation (17)), S_a is the design acceleration obtained for the code-defined approximate fundamental period $T_a = C_t \times h_n^x$ ($C_t = 0.073$ and $x = 0.75$ for steel BRBFs as per Table 12.8.1 of ASCE 7-16[1]), R was taken as 8 (as recommended for BRBFs as per Table 12.2.1 of ASCE 7-16[1]), I_e was assumed as 1, giving a base shear ratio $C_b = 0.2$, V_x is the storey shear, BRB V_x is the storey shear resisted by the BRBs (in this study 100%) and BRB V_{ix} is the storey shear resisted by each BRB as given in Table 2.

$$V = \frac{S_a W}{R / I_e}; \quad F_x = C_{vx} V; \quad C_{vx} = \frac{w_x h_x^{\,k}}{\sum_{i=1}^{n} w_i h_i^{\,k}} \quad (17)$$

Table 1. *L*60: Substructure model data.

(a) Storey heights and seismic weights

Storey	Height (m)	Weight (kN)
RFL	5	6064

(b) Section sizes ($\sigma_y = 325$ MPa)

Member	Section shape	Section size (mm)
Column	SHS	450 × 450 × 25

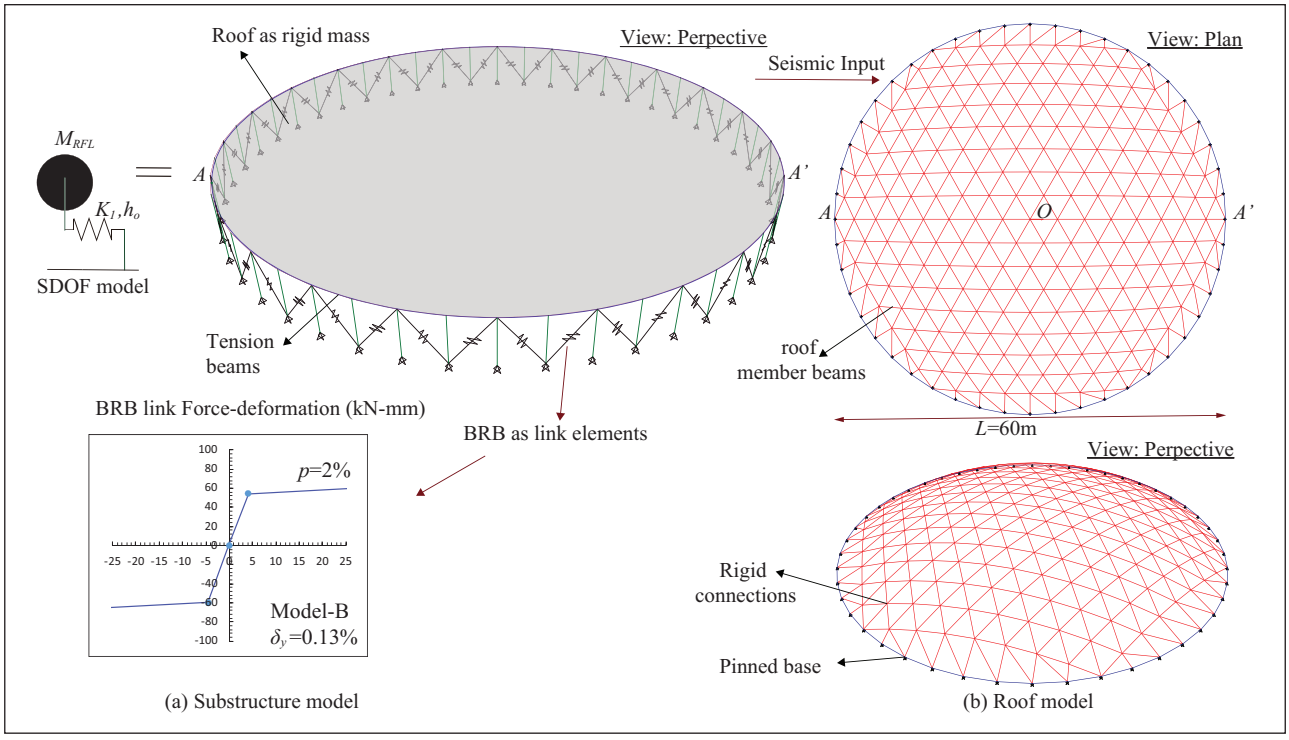

Figure 5. Single-storey substructure model and roof model: (a) Substructure model and (b) roof model.

Three combined models were designed to include substructures with different BRB design yield displacements. Note that for design of the substructure frame sections and the BRBs, the substructure models were adopted to represent the 3-d combined model as a lumped mass SDOF model shown in Figure 5(a). This idealisation enables the substructures of gridshell domes to be designed using the same code based simplified design procedures as prescribed for regular multistorey buildings. The substructure model for the Model-B (benchmark model) is shown in Figure 5(a) and was designed with a standard BRB yield drift ratio of 1/750.[34] A second model (Model-A) was designed for the same design base shear with a shorter BRB yield displacement of 0.06% such that the fundamental period is shorter and lies on the constant-acceleration region of the spectrum (Figure 7) and a third model (Model-C) was designed with a longer BRB yield displacement of 0.2% with the fundamental period in the constant-velocity region as given in Table 2. The axial force-displacement of BRBs were determined following the design guidelines by Takeuchi and Wada[34] and the BRB parameters are given in Table 2. In the analysis FE model, the BRBs have been modelled as links[35,36] with bilinear hysteretic characteristics and a post-yield stiffness ratio (p) of 2% typical of BRBFs.[34] However, in countries like Japan, due to the relatively cheap fabrication costs of moment-resisting frames (MRFs) using box columns and high-strength steel,[34] moment frames are often adopted as lateral-force resisting systems (also known as the dual systems) which remain elastic even after the dampers yield. Consequently, the post-yield stiffness of such substructures are much higher than those of BRBFs designed using pinned connections in the USA. Therefore, to investigate and validate the response estimation methods for such models with high post-yield stiffness, additional substructure models with $p = 10\%$ and 25% were created keeping the yield displacements the same across all models of the same series. The $p = 25\%$ models are representative of BRBF substructures in Japan[34] which adopt rigid moment connections in the supporting frames such that the stiffness provided by the damper to the stiffness of the supporting moment frame ratio (referred to as the 'K_d / K_f' ratio[34]) has a typical value of '$K_d / K_f = 3$'.[8,34] The $p = 10\%$ models are representative of substructures with post-yield stiffness in between the $p = 2\%$ and $p = 25\%$ models. These are typically seen in substructures without MRFs but with additional post-yield stiffness contributions from connections, gusset plates, and other non-structural components like the parapets. Additional models with $p = 0\%$ were also constructed to validate and confirm the approaches proposed for elastoplastic SDOF systems.

Roof model

The double-layered dome was designed for a span of 60 m and a half subtended angle (θ) of 30°. The lattice member sizes and vertical offsets (d) between the section centrelines are listed in Table 3. For simplicity, the

Table 2. Equivalent lateral forces: proportioning BRBs using $R = 8$.

Storey	h (m)	W_x (kN)	V_x (kN)	BRB V_x (kN)	BRB P_i (kN)	δ_y (mm)	BRB K_{eqi} (kN/m)	L_t (m)	σ_y (MPa)	A_c (mm^2)
Model-A ($T_1 = 0.3$s)										
RFL	5	6064	1061	1061	54	1.85	29160	6.4	90	600
Model-B ($T_1 = 0.4$s)										
RFL	5	6064	1061	1061	54	4.12	13125	6.4	235	230
Model-C ($T_1 = 0.5$s)										
RFL	5	6064	1061	1061	54	6.17	8748	6.4	235	230

A_c: area of core in plastic zone; K_{eqi}: equivalent axial stiffness; L_t: total BRB length; P_i: yield axial force; δ_y: yield axial deformation.[34]

Table 3. Roof models: member section sizes (σ_y = 325 MPa).

Model	Dead load (DL) (kPa)	Double-layer beam (mm)	Offset d (cm)	Single-layer beam (roof member) (mm)	m	Tension beam (mm)
L 60	2	$2 \times \phi$ 165.2 t 7.1*	150	ϕ 307.5 t 7.5*	50.1	ϕ 816 t 16

*ϕ = outer diameter; m = out-of-plane stiffness modification factor; t = thickness of circular hollow section.

double-layer lattice (Figure 5(b)) was modelled using equivalent beams with out-of-plane stiffness modification factors[16] with moment connections and pinning the roof lattice perimeter nodes. This dome model was used to identify the roof modes and is denoted as the 'roof model'. The fundamental period of the roof (T_R) was found to be 0.22 s with the roof exhibiting the anti-symmetric O1 mode shape.[7,13]

The combined analysis models were then constructed combining the roof model and substructure model. The design of roof members were checked by performing NLRHA analysis on the combined model using the load combination of 1.2DL + EQ (as per Section 2.3.6 of ASCE-7-16[1]) and ground motions specified in Figure 7 to check the member forces against their design strength as per the guidelines in AISC 360-16.[37] The roof geometry was modelled in *Grasshopper*[38] and imported to ETABS[35] for analysis. The roof member beams in ETABS were modelled as 'frame' objects which are general three-dimensional beam elements.[36]

The periods and mass participation of the first two modes (Γ_x in the direction of seismic input) of the combined model (Model-B) are shown in Figure 6. The first mode is the substructure T1 mode oscillating in-phase (labelled as 'O1 + T1') with the roof's dominant O1 mode.[7] The second mode exhibits the two modes oscillating out-of-phase (labelled as 'O1-T1') . This implies that only the O1 roof mode governs the dynamic response and the contribution of higher roof modes (like the O2, O2.5, or I mode is negligible). This is due to the fact that the substructure period ratio is long and therefore has interaction with only the roof's dominant O1 mode. The effects of substructure stiffness and period ratio on the dominant modes have been discussed in detail in previous studies.[7,16]

Input ground motions

11 natural ground motions were selected from the Pacific Earthquake Engineering Center strong motion database.[39] An initial suite was obtained using a standard search criteria of minimum magnitude of 6.5, a maximum magnitude of 7.5, and maximum shear velocity of 400 m/s. Eleven of the selected ground motions (Horizontal-1 direction) listed in Table 4 were then spectrally matched to the design spectrum (in accordance with Section 16.2 of ASCE 7-16[1]) such that the average of the spectra for the suite equals or exceeds 110% of the 5% target design spectrum over the period range of 0.2T1–1.5T1 where T1 was considered as 0.4 s (the fundamental period of benchmark Model-B). The response spectra of the 11 matched ground motions and the average of their spectra (labelled as 'Mean') are shown in Figure 7.

For NLRHA performed on the combined models using these spectral matched waves, Rayleigh damping of 5% was assigned to the first and second mode and the analysis was performed using the integration approach using the Hilber-Hughes-Taylor (HHT) method.[35,36] Two additional levels of ground motion intensity were considered to investigate the response at maximum-considered earthquake (MCE) level (1.5 × DBE level as prescribed by the ASCE-7[1]) and the serviceability level (SLE = 0.2 × the DBE level). As ASCE does not have a defined SLE design level, for this study, the SLE spectrum spectrum was defined by retaining the shape of the

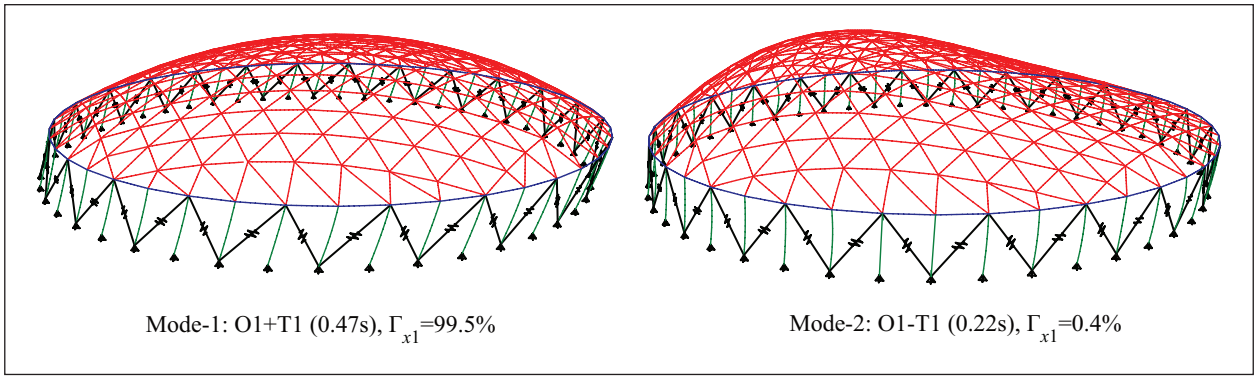

Figure 6. Model-B: combined model mode shapes.

Table 4. Input ground motions.

Ground motion no.	Earthquake*	Year	Station name	M	R_{jb} (km)	PGA (g)
1	Trinidad	1980	Rio Dell Overpass E-Ground	7.20	76.06	0.16
2	Spitak Armenia	1988	Gukasian	6.77	23.99	0.20
3	Loma Prieta	1989	Emeryville; Pacific Park	6.93	76.87	0.25
4	Loma Prieta	1989	Fremont – Emerson Court	6.93	39.66	0.19
5	Loma Prieta	1989	Hayward – BART Station	6.93	54.01	0.16
6	Loma Prieta	1989	Sunnyvale – Colton Ave	6.93	23.92	0.21
7	Northridge-01	1994	LA – 116th St School	6.69	36.39	0.21
8	Northridge-01	1994	LA – Baldwin Hills	6.69	23.50	0.24
9	Northridge-01	1994	LA – Cypress Ave	6.69	28.98	0.22
10	Northridge-01	1994	LA – N Faring Rd	6.69	12.42	0.28
11	Northridge-01	1994	LA – Obregon Park	6.69	35.43	0.36

M: moment magnitude; PGA: unscaled peak ground acceleration; R_{jb} : closest horizontal distance between the vertical projection of the rupture plane and recording station.
*These records were obtained from the NGA-West2 online ground motion database tool[39].

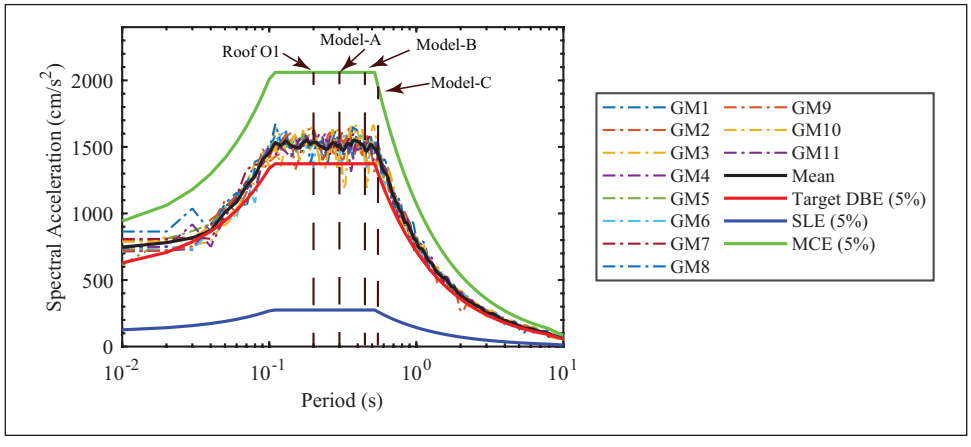

Figure 7. Target design spectrum and earthquake levels.

DBE spectra as is common practice in countries like Japan and New Zealand, and then scaling it by 0.2 (following the average ratio between the SLE and DBE design spectra of typical seismic codes as reviewed by Chandler and Duan[40]).

Comparison of peak substructure response

For each of the three substructure models, the elastic design spectral acceleration (S_{a1}) was used to obtain the elastic base shear (V_1) and then extrapolate the maximum

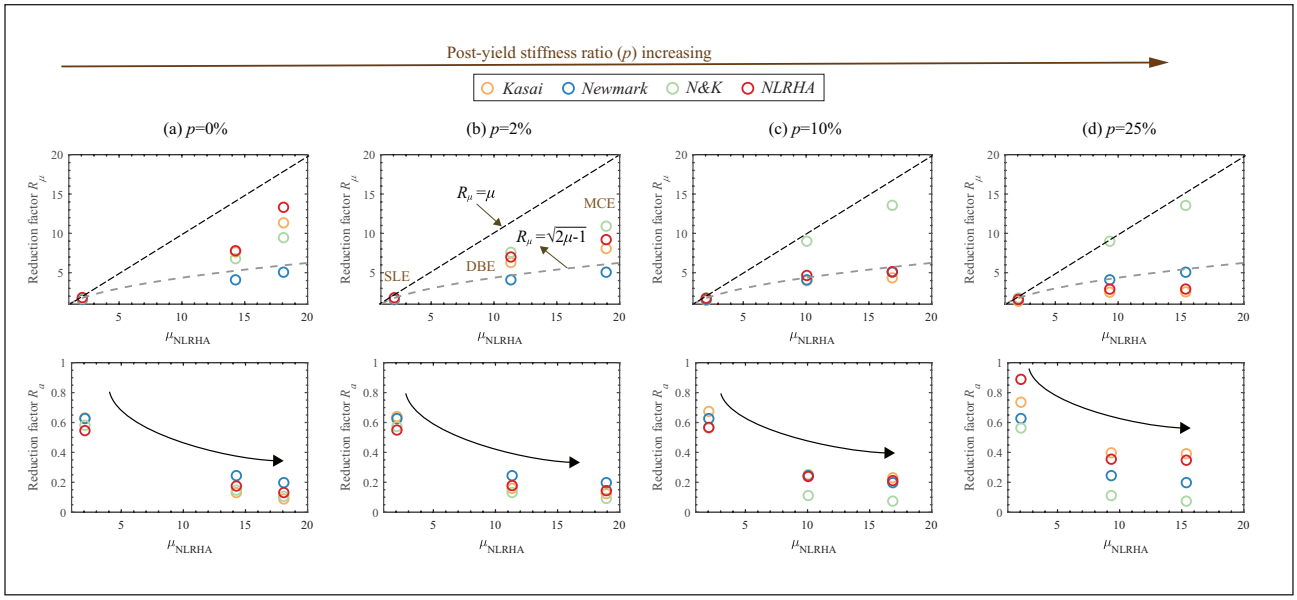

Figure 8. Single-storey Model-B: Reduction factors as functions of achieved displacement ductility: (a) $p = 0\%$, (b) $p = 2\%$, (c) $p = 10\%$, and (d) $p = 25\%$

elastic substructure roof displacement (D_1) at the substructure roof level (point A of Figure 5(a)) from the initial stiffness (K_1) as shown in equation (18). The maximum roof level acceleration (point A of Figure 5(a)) A_1 of the substructure is obtained from the corresponding roof displacement and the fundamental period and the response spectrum (S_{a1}) as shown in equation (18). The reduction factors (R_μ and R_a) were then computed following equations (2)–(4) from the target ductility μ_t using equations (7) and (19). For the equivalent linearisation approach, equations (8)–(16) were used. The mean responses obtained from the NLRHA performed on the combined models were also used to obtain the mean displacement ductility and reduction factor using equations (20) and (21).

$$V_1 = M_1 S_{a1} \quad D_1 = V_1 / K_1 \quad A_1 = D_1 \omega^2 \tag{18}$$

$$\mu_t = D_1 / D_y \tag{19}$$

$$\mu_{NLRHA} = D_{mean} / D_y \tag{20}$$

$$R_{\mu-NLRHA} = V_1 / V_{mean} \tag{21}$$

To compare the peak substructure responses from all the methods against the NLRHA results, the reduction in acceleration $R_a = A_{eq} / A_1$ and R_μ is plotted against the displacement ductility μ_{NLRHA} for Model-B in Figure 8. When the structure is subjected to SLE level earthquakes, the obtained ductility values are close to 2 with a small reduction in response. When the intensity of the earthquake is increased to DBE level, the mean ductility values increase to a range of 8–14 depending on the post-yield stiffness. For MCE levels, the values increase further to 15–20, but the reduction in response (R_a) is not linearly proportional to the increase in ductility. The results in Figure 8 exhibit a nonlinear relationship between R_μ and μ that is similar to the nonlinear R_μ and μ curve proposed by Newmark for short-period structures in Figure 4. The results also suggest that for short period structures, the actual ductility reduction factors (from NLRHA) do not strictly follow either the equal energy (equation (2)) or the equal displacement rule (equation (3)) but lie between the two Newmark factors as can be seen from the dotted lines in Figure 8(a) and (b). Therefore, for short-period models with low post-yield stiffness ($p < 10\%$), the Newmark method provides the most conservative estimates of the acceleration if compared to those obtained from the NLRHA.

For a detailed comparison between the two most conservative methods, the errors in estimation of the response against the NLRHA response for the DBE levels have been shown in Table 5. As the post-yield stiffness increased, the reduction ratio R_a obtained from the NLRHA and Kasai method increased but the R-factor methods estimated lower peak accelerations assuming an elastoplastic response. However, as the Newmark method is conservative for short-period structures with elastoplastic response (with 39% overestimation of the R_a value for $p = 0\%$ in

Table 5. Single-storey Model-B: Errors in estimation of DBE response against the NLRHA response.

Method	% error in R_μ estimation				% error in R_a estimation			
	p = 0%	p = 2%	p = 10%	p = 25%	p = 0%	p = 2%	p = 10%	p = 25%
Newmark	–47	–41	–12	+40	+39	+37	+2	–31
Kasai	−2	–10	–14	–13	–25	–10	+5	+12

+ ve % error indicates the estimated value is more than the NLRHA value and vice-versa.

Table 6. Single-storey models: Kasai method's equivalent linearisation results, p = 2%.

	h_{o1}	h_{eq1}	K_{eq1} / K_1	D_h	R_d	R_a	μ_{t1}	T_1	T_{eq1}	T_R
Model-B-SLE	0.05	0.12	0.58	0.75	1.11	0.64	1.77	0.45	0.59	0.23
Model-B-DBE	0.05	0.44	0.10	0.43	1.55	0.16	8.87	0.45	1.41	0.23
Model-B-MCE	0.05	0.47	0.07	0.42	1.90	0.12	13.31	0.45	1.77	0.23

Table 5), the Newmark method remained conservative for models with higher post-yield stiffness as well (Figure 8(b) and (c) and Table 5). As the post-yield stiffness further increased to 25%, the Newmark method estimates became unconservative with the error increasing to 31%. This confirms that even though Newmark method has been proposed for elastoplastic systems, it may be applied for short-period structures with post-yield stiffness of up to 10%. Finally, among the discussed estimation methods, Kasai's approach (Table 6) provides the most accurate estimate of the response to that obtained from NLRHA for all cases as this approach is more mathematical and less empirical, making it applicable to any bilinear system. The actual ductility values and damping ratios are estimated, leading to better accuracy in response estimation.

Peak roof response

Substructure T1 mode amplification factors

The substructure-roof interactions for single-storey structures are defined by the amplification factors F_{H1} and F_{V1}[7] that depend on the mass (R_M) and period (R_T) ratios[7] given in equation (22). These are characterised as ratios of the effective modal mass (M_{eq}) and fundamental period (T_1) of the substructure model, which includes the roof mass, relative to the total roof mass (M_R), and period of the (dominant) fundamental roof O1 mode (T_R).[7,16] The mass ratios increase as the substructure gets heavier (such as in the case of an RC substructure which tends to be much heavier than a steel frame counterpart). Similarly, the period ratios may decrease as the substructure becomes stiffer (such as when the substructure frame sizes increase).[16] Such heavy substructures with $R_{T1} < 1.5$ and $R_M > 2$ produce higher amplification between the T1 and O1 modes due to resonance, as noted by Takeuchi et al.[7] To account for this resonance induced amplification, the amplification factors have been modified to $F_H^{'}$ and $F_V^{'}$ (when $R_{T1} < 1.5$ and $R_{M1} > 2$), as given by equations (25) and (26).[7]

The proposed amplification factors F_{H1} and F_{V1} are defined by equations (23)–(26).[7] A vertical calibration factor $C_v\theta$ (equation (24)) of 1.85θ was adopted as previously proposed based on a numerical study investigating the influence of the half-subtended angle on the peak vertical acceleration.[7] After obtaining the peak substructure response ${}_sA_{Heq}$, the peak roof accelerations of the combined model ${}_cA_H$ and ${}_cA_V$ are estimated using the amplification factors and the dominant roof O1 mode shape adopted for the envelope, which has the horizontal and vertical distributions given by equations (27) and (28),[7] where x and y are the coordinates of roof nodes, the roof centre is located at $\{x, y\} = \{0,0\}$ and L is the span of the dome. Note that in this paper, the preceding subscripts r, s, and c refer to the roof, substructure, and combined models, respectively.

$$R_M = \frac{{}_sM_{eq}}{{}_rM_R}, \quad R_{T1} = \frac{{}_sT_1}{{}_rT_R} \tag{22}$$

$$F_{H1} = \begin{Bmatrix} 3 & (0 < R_{T1} \le 5/36) \\ \sqrt{5/(4R_{T1})} & (5/36 < R_{T1} \le 5/4) \\ 1 & (5/4 < R_{T1}) \end{Bmatrix} \tag{23}$$

$$F_{V1} = \begin{Bmatrix} 3C_V\theta & (0 < R_{T1} \le 5/16) \\ (\sqrt{5/R_{T1}} - 1)C_V\theta & (5/16 < R_{T1} \le 5) \\ 0 & (5 < R_{T1}) \end{Bmatrix} \tag{24}$$

$$F_{H1}^{'} = \sqrt{F_{H1}{}^2 + \frac{1}{(1 - R_{T1}{}^2)^2 + (1/R_{M1})^\theta}} \tag{25}$$

$$F_{V1}^{'} = \sqrt{{F_{V1}}^2 + \frac{1}{(1-{R_{T1}}^2)^2 + (1/R_{M1})}} \quad (26)$$

$${}_c A_{Hi}(x,y) = {}_s A_{Heqi}\{1 + (F_{Hi} - 1)\cos\frac{\pi\sqrt{x^2+y^2}}{L}\} \quad (27)$$

$${}_c A_{Vi}(x,y) = {}_s A_{Veqi} F_{Vi} \frac{x}{\sqrt{x^2+y^2}} \sin\frac{2\pi\sqrt{x^2+y^2}}{L} \quad (28)$$

In previous studies,[13,18] for the Kasai's equivalent linearisation approach, the period ratios were computed using the substructure's inelastic periods R_{Teq1}[13] and the rationale behind this assumption has not been confirmed yet. Therefore, to investigate the relationship between the amplification factors and the inelastic period ratios, the vertical amplification factors computed from the mean NLRHA response divided by the peak substructure acceleration $F_V = {}_c A_{Vmax} / {}_s A_{Heq}$ have been plotted against the elastic (R_{T1}) and inelastic (R_{Teq1}) period ratios (equation (29)).

$$R_{T1} = \frac{{}_s T_1}{{}_r T_R}; \quad R_{Teq1} = \frac{{}_s T_{eq1}}{{}_r T_R} \quad (29)$$

It was observed that the obtained amplification factors plotted against the elastic period ratios (Figures 9(a) and 10(a)) are in better agreement as opposed to the plots against the inelastic period ratios (Figures 9(b) and 10(b)). The largest errors between the proposed curves and the obtained factors were observed for the $p = 2\%$ and $p = 10\%$ models as can be seen in Figure 9(b). As the post-yield stiffness increases, the more conservative the proposed factor becomes. The horizontal amplification factors have also been plotted for comparison as $F_H = {}_c A_{Hmax} / {}_s A_{Heq}$. In case of horizontal amplification, the errors in the calculation remain the same as the horizontal amplification factor becomes constant at 1 ($F_{H1} = 1$) for all period ratios larger than 1.25 ($R_{T1} > 1.25$). Therefore, in this study, the more accurate elastic period ratios (equation (22)) are adopted for the computation of the amplification factors.

Direct-R method

The 'Modal response spectrum analysis' method in ASCE-7-16[1] recommends calculation of design level force-related parameters by dividing the elastic response directly by R/I_e (=8 in this study). Therefore, another straightforward method of estimating the DBE-level response is to divide the peak elastic roof response directly by the R-factor as shown in equation (30). However, there is no explicit commentary on modification of this factor for models with post-yield stiffness. Furthermore, employing a single reduction factor for all modes to estimate the peak accelerations may underestimate the overall response as the actual reduction in acceleration depends on the achieved target ductility and additional modal damping. The higher substructure modes may not achieve such high levels of ductility as assumed in this approach. In addition, since the method is fundamentally derived from the 'equal-displacement rule' (assuming the structures are in the constant-velocity region), the applicability of this method to models with fundamental periods in the constant-acceleration region (or short-period range) has not been proven yet. Therefore, to illustrate the applicability of this method, it is also used for computing DBE level response (using a reduction factor of $R = 8$) for comparison and is labelled as the 'Direct-R' method hereon.

$$R_a = \frac{1}{R} \quad (30)$$

Comparison of peak roof response

The peak roof accelerations for the Model-A, Model-B and Model-C were calculated using the first mode amplification factors in equations (23)–(28). For the equivalent linearisation approach, ${}_s A_{Heqi}$ was computed considering the effect of both the period shift and the damping[13] using equations (8)–(16). For the R-factor approach methods, the peak substructure acceleration was obtained using equation (7). The proposed ridgeline *A-O-A′* (Figure 5) accelerations are compared with the mean NLRHA results in Figures 11 and 12.

When the post-yield stiffness ratio (p) is low (Figure 11), the peak substructure accelerations for Model-C in the constant velocity region obtained from the Newmark and N&K method were nearly equal to the peak accelerations obtained from Kasai's method leading to similar accuracy in the overall roof response. Model-A exhibited the largest amplifications in both the horizontal and vertical directions as the substructure periods were closest to the roof's period (smallest period ratio R_T) among the three models. In small ductility regions (Figure 11 SLE results), all methods give reasonably accurate results. In large ductility regimes like the DBE and MCE levels, for structures with fundamental periods in the constant velocity region (Model-C), all R-factor methods estimate the DBE response with reasonable accuracy although the Kasai method is the most conservative, and the Newmark method presents the most conservative response estimates for models in the constant acceleration region (Model-A and Model-B). The differences in the Newmark and Kasai methods may further be understood by considering the example of Models A and B and their MCE response in Figure 11(a) and (b). Both models have periods in the constant acceleration region and therefore have the same

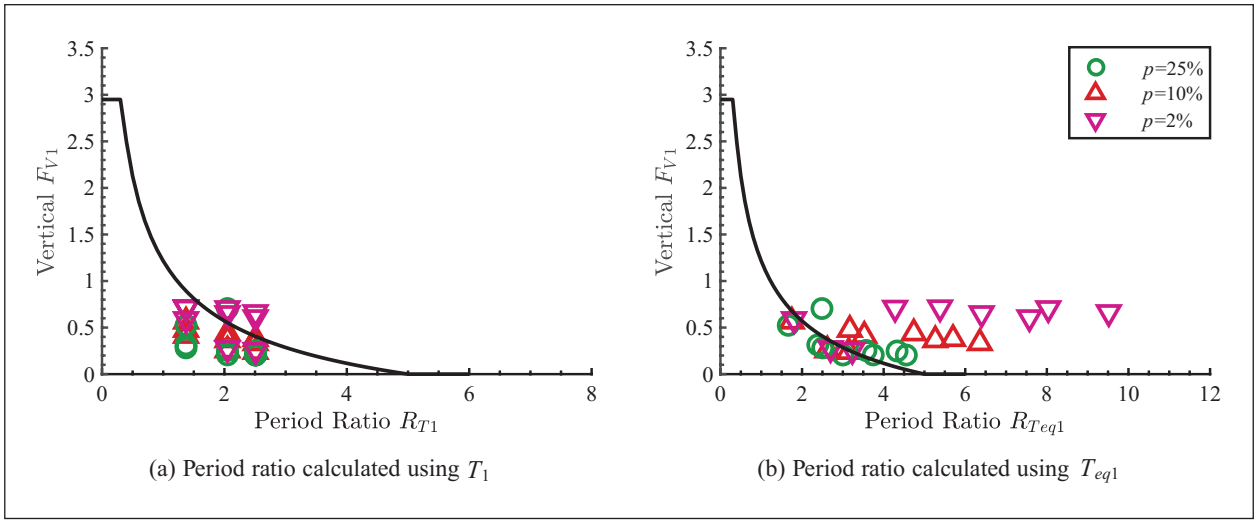

Figure 9. Vertical amplification factors w.r.t period ratios: (a) period ratio calculated using T_1 and (b) period ratio calculated using T_{eq1}.

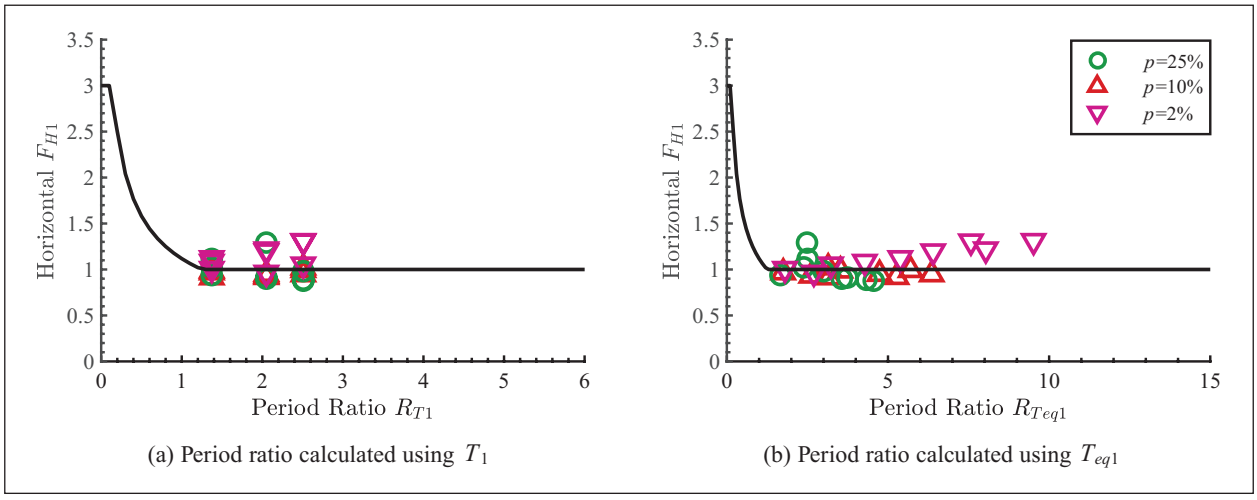

Figure 10. Horizontal amplification factors w.r.t period ratios: (a) period ratio calculated using T_1 and (b) period ratio calculated using T_{eq1}.

horizontal elastic accelerations ($A_1 \approx 23\,\text{m/s}^2$). In addition, both models have nearly the same target ductility value for MCE levels ($\mu_t \approx 13$), and so the Newmark method gives $R_\mu = 5$ (following equation (2)) for both models resulting in identical peak substructure acceleration ($A_{Heq1} \approx 4.5\,\text{m/s}^2$ as can be seen from the 'Newmark' horizontal response). However, the A_{Heq1} from the NRLHA and Kasai method differ for the two models. This illustrates the shortcoming of the Newmark method which considers the effect of ductility while the effect of energy dissipation is implicitly accounted for by the backbone elastoplastic curve using the equal energy rule, and therefore may not always be accurate in estimating the maximum response values. The iterative equivalent linearisation approach better captures the energy dissipation by considering the equivalent viscous damping as well as the effect of period elongation which is quantified in equations (13)–(15) by the Kasai method[20,21] and is different in the two models.

When the post-yield stiffness ratio (p) is large (Figure 12), the peak substructure accelerations for all models were underestimated by the Newmark and the N&K method (Figure 8). These errors increase as the level of the intensity increases from SLE to MCE. In addition, all methods give reasonably accurate results in small ductility regions (Figure 12 SLE results) as the structure is largely in the elastic range. As observed for the low post-yield ratio models, Model-A exhibited the largest amplifications in both the horizontal and vertical directions. Kasai's relatively rigorous equivalent linearisation method accurately estimates the substructure response (Figure 8) and therefore presents

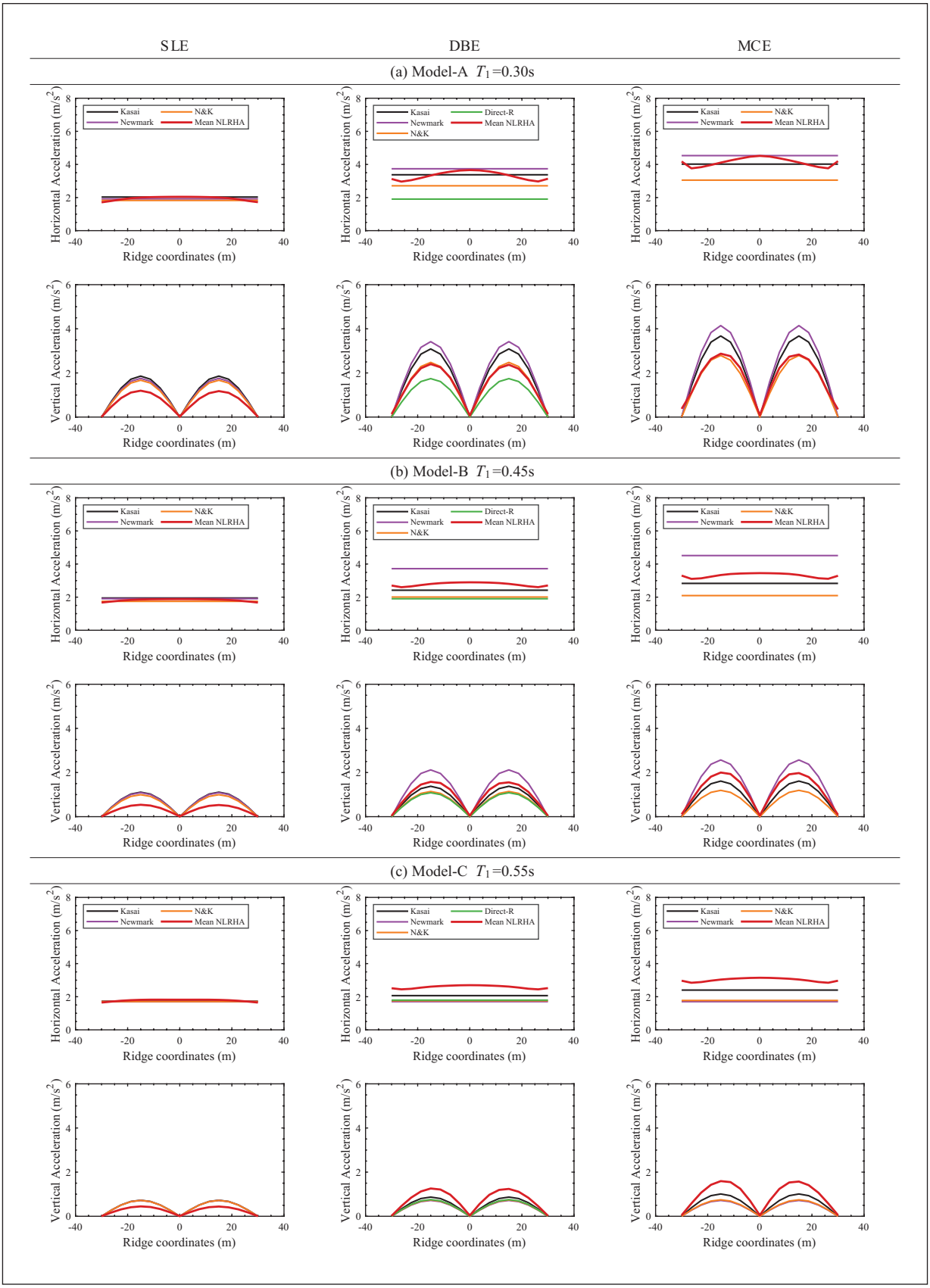

Figure 11. Roof ridgeline accelerations (post-yield stiffness ratio $p = 2\%$): (a) Model-A $T_1 = 0.30$ s, (b) Model-B $T_1 = 0.45$ s, and (c) Model-C $T_1 = 0.55$ s.

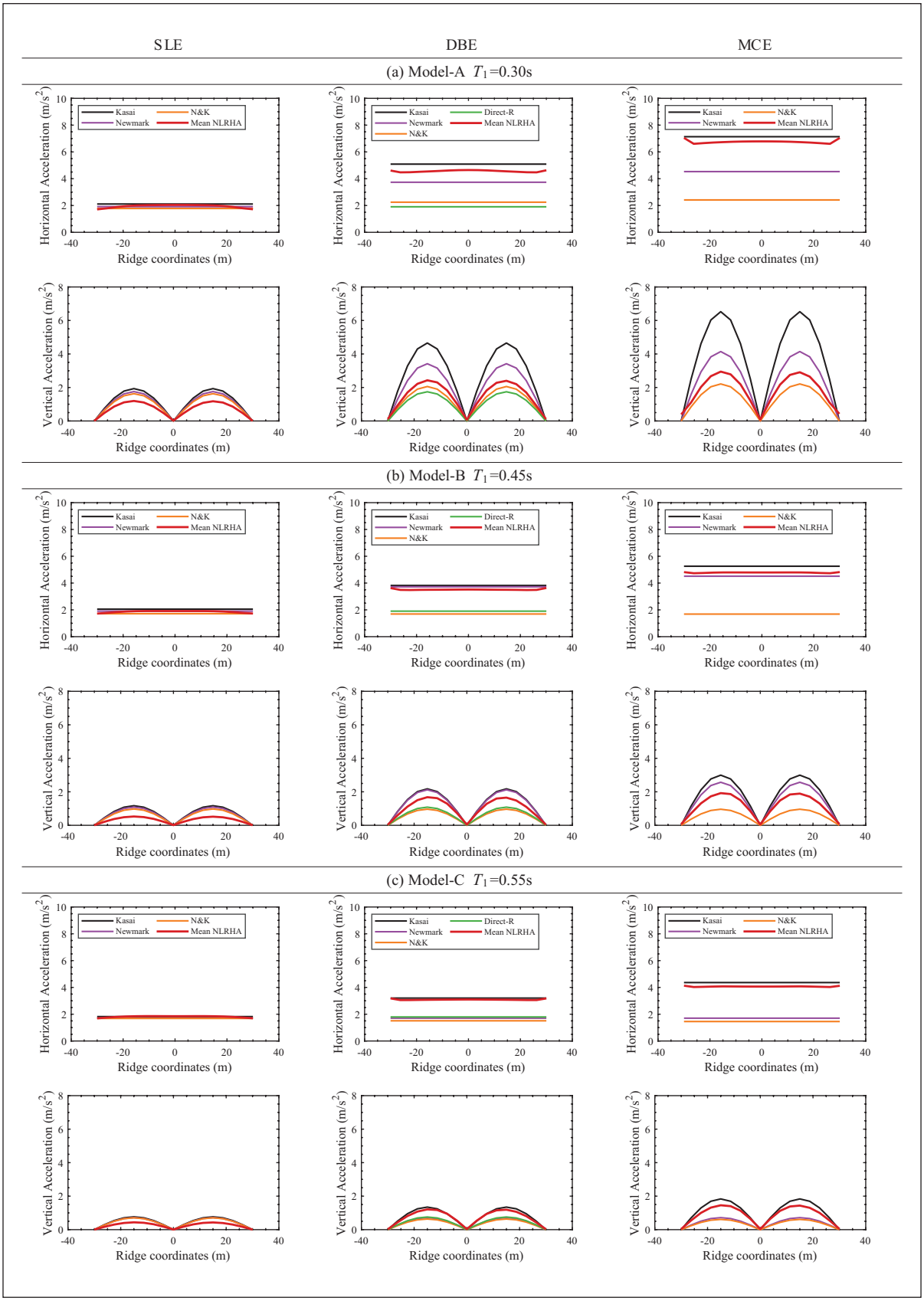

Figure 12. Roof ridgeline accelerations (post-yield stiffness ratio $p = 10\%$): (a) Model-A $T_1 = 0.30$ s, (b) Model-B $T_1 = 0.45$ s, and (c) Model-C $T_1 = 0.55$ s.

a conservative roof response envelope (Figure 12) for models in both the constant acceleration and velocity regions. It is therefore recommended to use the equivalent linearisation approach when p is higher than 2%.

Effect of higher substructure modes

2-storey analysis models

To investigate the applicability of the approach of using R-factors for substructures with higher modes, the single-storey substructure was replaced with a two-storey substructure. As in the single-storey models, the first storey and the roof level are each 5 m high and the first storey has a floor weight of 7 kPa and the roof dead load is assumed to be 2 kPa (Table 3). The substructure model is shown in Figure 13 and the gravity frame section sizes are also adopted from the single-storey model given in Table 7. The BRBs for the 2-storey substructure models were designed using the same design procedure as for single-storey models (using equation 17) and the properties of the BRBs and design storey shears are given in Table 8. The combined analysis models A, B and C were then constructed combining the roof model (Figure 5(b)) and the substructure models (Figure 13).

The seismic response of domes with multistorey substructures may be interpreted as a combination of responses from both T1-roof and T2-roof interactions.[16] The contribution of each of these modes to the overall response is directly proportional to their mass participation values. Note that T2 includes all of the translational modes with a single inflection point, while T1 refers to the translational sway modes. However, T1 or T2 modes about all axes have identical periods for the dome models considered in this study due to symmetry.[16] Unlike the single-storey cases, both the substructure T1 and T2 modes interact with the nearest roof mode. The substructure periods and roof periods are mapped on the design spectrum in Figure 14. Model-B and Model-C have fundamental periods (first substructure mode (T1)) in the constant velocity region, and Model-A with a stiffer substructure has a relatively shorter fundamental period in the constant acceleration region. The fundamental periods (T1) for all models contribute to a mass participation ratio (in the direction of seismic input i.e. the x-direction) of about 90% and the remaining 10% came from the higher T2 mode which lies in the constant acceleration region for all models. This implies a higher spectral acceleration value from the T2 modes. The substructure T2 modes are also in close proximity to roof's dominant O1 and O2 modes giving rise to second mode period ratios $R_{T2} = T_2 / T_R$ in the range of 1 (where T_2 is the substructure T2 mode period and T_R is the roof's O1 mode as defined previously by the authors[16]). Consequently, in these models, the vertical amplification factors quantifying the T2-roof interactions are larger and more significant than those from the T1-roof interactions with the longer R_{T1} period ratios.[16]

2-storey model: Inter-storey drifts

The mean peak substructure inter-storey drifts and mean residual inter-storey drifts obtained from NLRHA for the combined models are given in Figure 15. For structures having four stories or less, ASCE-7[1] prescribes an allowable storey drift of 2.5% for DBE level. The obtained mean storey drifts are within the permissible ASCE limits for all models. Typical values of mean residual drift are about 0.3% for $p = 2\%$ models under the DBE level. These values increase to 0.6% under the MCE level. If 0.5% residual drift is assumed to be the limit beyond which the structures are no longer practically usable,[41] then the models with less than or equal to 2% post-yield stiffness ratio may not meet this immediate occupancy performance level under MCE level excitation.

2-storey models: Peak substructure response

For each of the three substructure models, modal pushover analyses corresponding to the first and second translational modes were performed (Figure 16) to obtain the initial base shear to roof displacement stiffness (K_{1i}) as shown in equation (18). The elastic design spectral accelerations of the first and second modes (S_{a1} and S_{a2}) were used to obtain the elastic base shears (V_i) and then extrapolate the maximum elastic substructure roof displacement (D_i) at point A of Figure 13(a) from the initial stiffness (K_{1i}) as shown in equation (18). The peak elastic RFL level acceleration A_i of the substructure is also obtained from the corresponding roof displacement and the fundamental period and the response spectrum as shown in equation (18). The reduction factors ($R_{\mu i}$ and R_{ai}) were then computed for both T1 and T2 modes following equations (2)–(4) from the target ductility μ_{ti} using equations (7) and (19). For the equivalent linearisation approach, equations (8)–(16) were used. The peak inelastic base shear and roof acceleration of the substructure model were then obtained by combining the modal base shears using the SRSS modal combination rule using equations (31) and (32).

$$ {}_sV = \sqrt{\left(\frac{V_1}{R_{\mu 1}}\right)^2 + \left(\frac{V_2}{R_{\mu 2}}\right)^2} \tag{31} $$

$$ {}_sA_{eq} = \sqrt{\left(\frac{A_1}{R_{\mu 1}}\right)^2 + \left(\frac{A_2}{R_{\mu 2}}\right)^2} \tag{32} $$

The peak substructure accelerations ${}_sA_{eq}$ and base shear ratio C_b ($= {}_sV / W$ where W is the seismic weight)

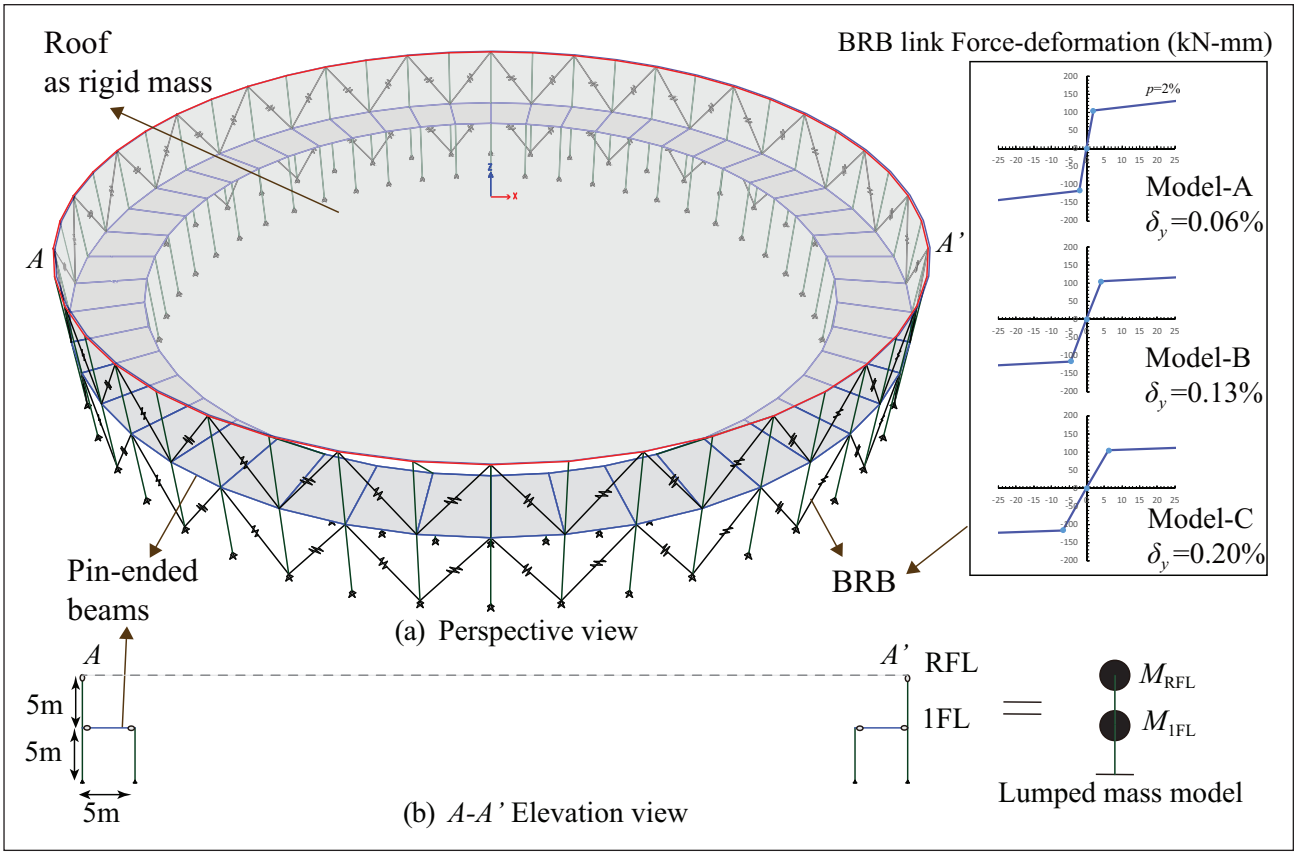

Figure 13. 60 m 2-storey substructure model and modelling assumptions: (a) perspective view and (b) A-A′ elevation view.

Table 7. 2-storey substructure model data.

(a) Storey heights and seismic weights			(b) Section sizes		
Storey	Height (m)	Weight (kN)	Member	Section shape	Section size (mm)
RFL	10	6064	Column	SHS	450 × 450 × 25
1FL	5	6032	Beam	I beam	340 × 250 × 9 × 14

Table 8. 2-storey model: Equivalent lateral forces for proportioning BRBs (σ_y = 235,205 MPa).

Storey	h (m)	W_x (kN)	V_x (kN)	BRB V_x (kN)	BRB V_{ix} (kN)	BRB P_i (kN)	δ_y (mm)	BRB K_{eqi} (kN/m)	A_c (mm^2)
Model-A (T_1 = 0.38s, T_2 = 0.15s)									
RFL	10	6064	1414	1414	40	70	1.85	37770	341
1FL	5	6032	2117	2117	60	105	1.85	56558	511
Model-B (T_1 = 0.56s, T_2 = 0.23s)									
RFL	10	6064	1414	1414	40	70	4.12	16997	298
1FL	5	6032	2117	2117	60	105	4.12	25451	446
Model-C (T_1 = 0.69s, T_2 = 0.28s)									
RFL	10	6064	1414	1414	40	70	6.17	11331	298
1FL	5	6032	2117	2117	60	105	6.17	16967	446

A_c : area of core; K_{eqi} : BRB equivalent axial stiffness; P_i : yield axial force in each BRB; δ_y : yield axial deformation; as defined in Takeuchi and Wada[34].

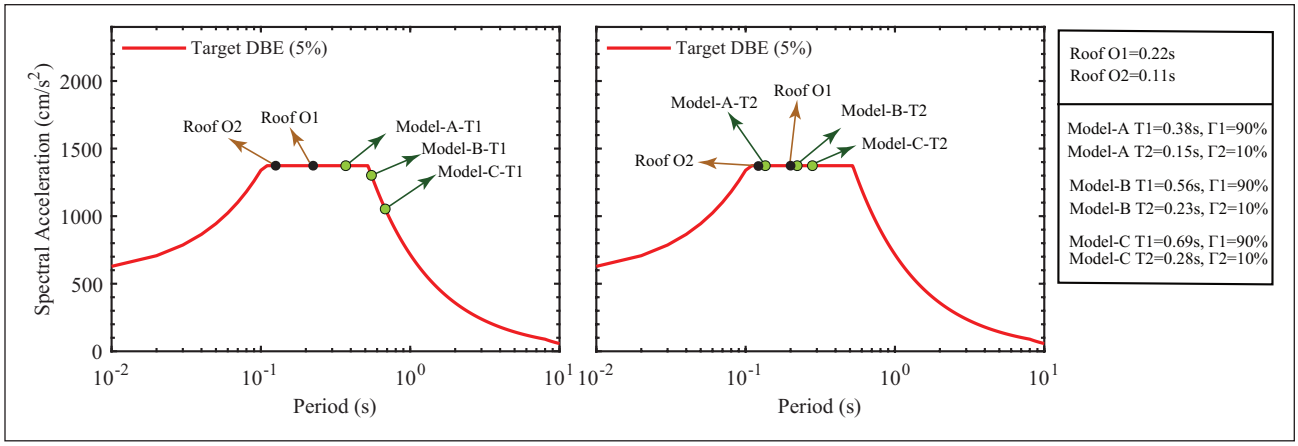

Figure 14. 2-storey models: Substructure and roof periods on the design acceleration spectrum.

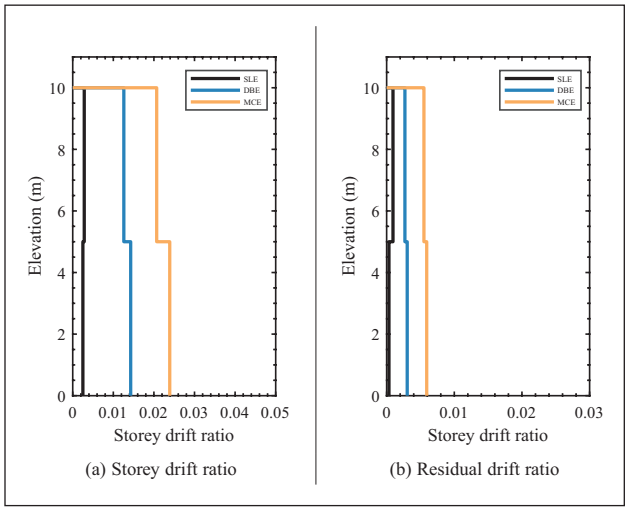

Figure 15. 2-storey Model-B $p = 2\%$: mean of peak storey drift ratios of substructure: (a) storey drift ratio and (b) residual drift ratio.

for all the models are compared with the mean NLRHA response in Figure 17. The typical DBE level base shear ratios are low at around 0.3 and increase to 0.35 for MCE level for $p = 2\%$ models. These values further increase with increasing post-yield stiffness with Model-A with the lowest reduction and the highest base shear ratio at about 0.9. As observed for the single-storey models, the R-factor methods estimate the base shear and accelerations with good accuracy for $p = 2\%$, with Newmark's method being the most conservative of all the estimation methods in the short-period range. As the post-yield stiffness ratio increases ($p = 25\%$), Kasai method is the most accurate if compared with the mean NLRHA response. For SLE level response and low-ductility regimes, all methods are equally accurate.

The achieved damping, reduction ratios and the periods corresponding to Kasai's evaluation method are also shown in Tables 8 to 12. To compare the reduction in acceleration for each mode across models with different post-yield stiffness, the reduction in peak substructure acceleration $R_{ai} = A_{eqi} / A_i$ obtained from the Kasai method is plotted for modes T1 and T2 for Model-A, Model-B and Model-C in Figure 18. For models with $p = 2\%$, the reduction in T1 mode is the lowest for the SLE level with typical R_{a1} values at around 0.7. These values reduced further to 0.2 for the DBE level and 0.1 for MCE level. As the post-yield stiffness increases to $p = 10\%$, the reduction ratio increases to 0.3 for the DBE level and 0.2 for the MCE level. The models with $p = 25\%$ therefore exhibit the lowest reductions in acceleration with typical R_{a1} values at around 0.8 for the SLE level, 0.4 for the DBE level and 0.3 for the MCE level. However, for the T2 mode response, the increase in post-yield stiffness has a relatively minor effect on the reduction ratios as the additional damping is lesser and the ductility values are smaller in the higher mode (Tables 10 and 12). Thus, substructures designed with a high post-yield stiffness can achieve reduced residual inter-storey drifts (Figure 23(b)) but the corresponding grid-shell roofs may have to be designed for higher design forces due to the increased seismic input.

2-storey models: Peak roof response

The multistorey structures have been previously found to exhibit significantly higher amplification, especially in the vertical direction for $R_{T1} > 2$ [16] which may be attributed to the substructure T2 mode and its interaction with the roof's predominant modes in its close proximity. To account for these higher-mode effects, the T2-roof horizontal and vertical amplification factors were proposed[16] as a function of the period ratio R_{T2} as defined in equations (33) and (34). After obtaining the peak substructure response, the peak roof accelerations for the combined models were calculated for each of the modes

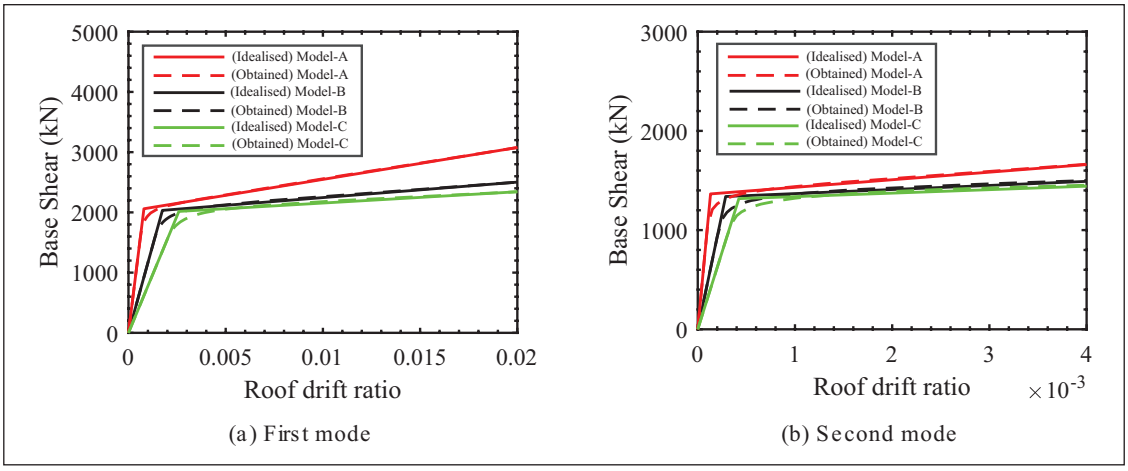

Figure 16. Modal pushover curves and idealisation of structural response (p = 2% 2-storey models): (a) first mode and (b) second mode.

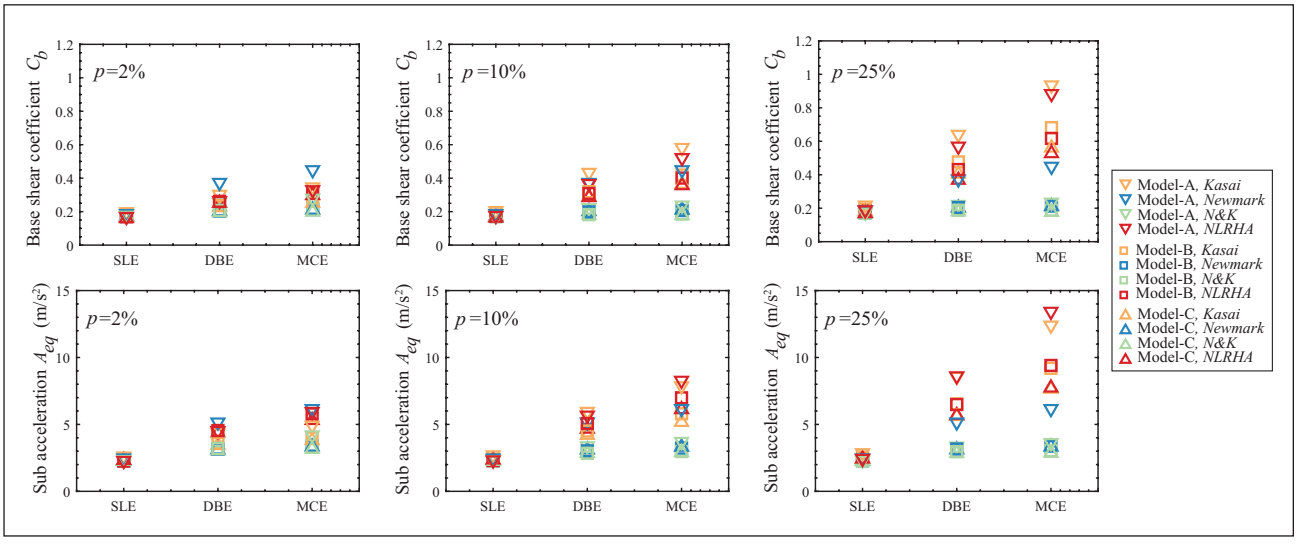

Figure 17. 2-storey models: Base shear ratios and peak substructure (RFL) acceleration.

Table 9. p = 2% 2-storey models: peak substructure first-mode (T1) parameters.

	h_{eql}	K_{eql} / K_l	D_h	R_d	R_a	μ_{tl}	T_l	T_{eql}	T_R
Model-A-SLE	0.10	0.62	0.79	1.14	0.71	1.63	0.38	0.48	0.23
Model-A-DBE	0.43	0.11	0.44	1.74	0.20	8.14	0.38	1.12	0.23
Model-A-MCE	0.47	0.07	0.42	2.15	0.15	12.21	0.38	1.41	0.23
Model-B-SLE	0.09	0.65	0.82	1.01	0.66	1.53	0.56	0.69	0.23
Model-B-DBE	0.42	0.12	0.44	1.25	0.16	7.66	0.56	1.59	0.23
Model-B-MCE	0.46	0.08	0.43	1.52	0.12	11.48	0.56	2.00	0.23
Model-C-SLE	0.07	0.78	0.92	1.04	0.81	1.24	0.69	0.77	0.23
Model-C-DBE	0.38	0.16	0.46	1.14	0.19	6.18	0.69	1.70	0.23
Model-C-MCE	0.44	0.10	0.43	1.36	0.14	9.27	0.69	2.15	0.23

Table 10. $p = 2\%$ 2-storey models: peak substructure second-mode (T2) parameters.

	h_{eq2}	K_{eq2}/K_2	D_h	R_d	R_a	μ_{t2}	T_2	T_{eq2}	T_R
Model-A-SLE	0.05	1.00	1.00	1.00	1.00	1.00	0.15	0.15	0.23
Model-A-DBE	0.08	0.73	0.88	1.12	0.82	1.37	0.15	0.18	0.23
Model-A-MCE	0.15	0.49	0.69	1.19	0.58	2.06	0.15	0.22	0.23
Model-B-SLE	0.05	1.00	1.00	1.00	1.00	1.00	0.23	0.23	0.23
Model-B-DBE	0.08	0.72	0.87	1.12	0.81	1.40	0.23	0.27	0.23
Model-B-MCE	0.16	0.49	0.68	1.18	0.57	2.10	0.23	0.33	0.23
Model-C-SLE	0.05	1.00	1.00	1.00	1.00	1.00	0.28	0.28	0.23
Model-C-DBE	0.08	0.71	0.86	1.13	0.80	1.42	0.28	0.33	0.23
Model-C-MCE	0.16	0.47	0.67	1.20	0.57	2.13	0.28	0.41	0.23

Table 11. $p = 25\%$ 2-storey models: peak substructure first-mode (T1) parameters.

	h_{eq1}	K_{eq1}/K_1	D_h	R_d	R_a	μ_{t1}	T_1	T_{eq1}	T_R
Model-A-SLE	0.09	0.71	0.84	1.09	0.78	1.63	0.38	0.45	0.23
Model-A-DBE	0.21	0.34	0.60	1.33	0.45	8.14	0.38	0.65	0.23
Model-A-MCE	0.19	0.31	0.62	1.45	0.44	12.20	0.38	0.68	0.23
Model-B-SLE	0.08	0.74	0.86	1.01	0.74	1.53	0.56	0.65	0.23
Model-B-DBE	0.21	0.35	0.61	1.03	0.36	7.65	0.56	0.95	0.23
Model-B-MCE	0.20	0.31	0.62	1.11	0.34	11.48	0.56	1.01	0.23
Model-C-SLE	0.06	0.84	0.94	1.03	0.86	1.24	0.69	0.75	0.23
Model-C-DBE	0.20	0.37	0.61	0.99	0.37	6.18	0.69	1.12	0.23
Model-C-MCE	0.20	0.33	0.61	1.06	0.35	9.27	0.69	1.20	0.23

Table 12. $p = 25\%$ 2-storey models: peak substructure second-mode (T2) parameters.

	h_{eq2}	K_{eq2}/K_2	D_h	R_d	R_a	μ_{t2}	T_2	T_{eq2}	T_R
Model-A-SLE	0.05	1.00	1.00	1.00	1.00	1.00	0.15	0.15	0.23
Model-A-DBE	0.07	0.79	0.91	1.09	0.86	1.37	0.15	0.17	0.23
Model-A-MCE	0.12	0.60	0.76	1.11	0.67	2.06	0.15	0.20	0.23
Model-B-SLE	0.05	1.00	1.00	1.00	1.00	1.00	0.23	0.23	0.23
Model-B-DBE	0.07	0.79	0.90	1.08	0.85	1.40	0.23	0.26	0.23
Model-B-MCE	0.13	0.61	0.74	1.08	0.66	2.10	0.23	0.29	0.23
Model-C-SLE	0.05	1.00	1.00	1.00	1.00	1.00	0.28	0.28	0.23
Model-C-DBE	0.07	0.76	0.90	1.11	0.84	1.42	0.28	0.32	0.23
Model-C-MCE	0.12	0.56	0.75	1.16	0.65	2.13	0.28	0.37	0.23

from the inelastic response ${}_s A_{Heqi}$ and the corresponding first and second mode amplification factors in equations (23)–(28). For the equivalent linearisation approach, the substructure's peak modal response ${}_s A_{Heqi}$ was computed considering the effect of both the period shift and the damping.[13] For the R-factor approach methods, the peak inelastic substructure acceleration for each mode was obtained using equation (7). For comparison, the DBE level response was also computed using the Direct-R method and a reduction factor $R = 8$ for both the modes.

The modal accelerations at each node were then combined using equations (35) and (36) to obtain the combined response envelope. This study uses an absolute summation rule.[13,16] The equivalent static seismic forces for each node may then be computed from the nodal mass m_k and acceleration ${}_c A_H(x, y)$ or ${}_c A_V(x, y)$ at position (x, y) using equation (37).

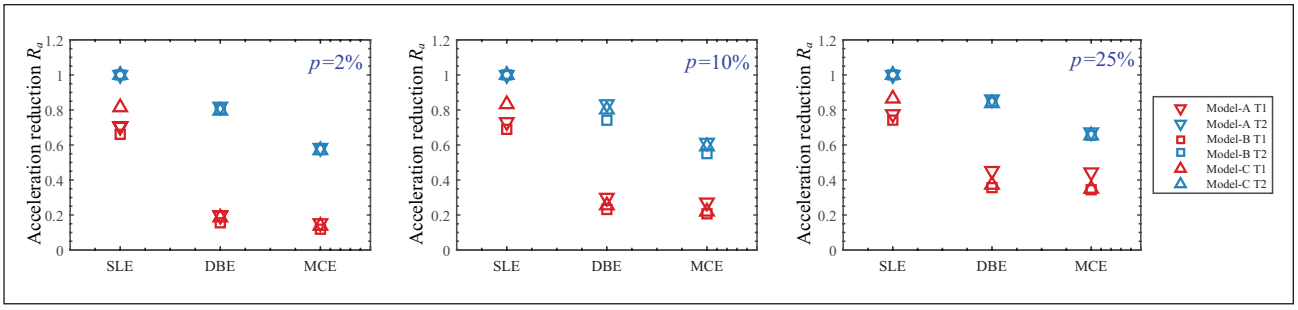

Figure 18. Kasai method: reduction in 2-storey substructure modal acceleration.

$$F_{H2} = 1 \tag{33}$$

$$F_{V2} = \begin{cases} 0 & R_{T2} \le 1/5 \\ 6C_V\theta(R_{T2} - 1/5) & 1/5 < R_{T2} < 7/10 \\ 3C_V\theta & 7/10 \le R_{T2} \le 21/16 \\ \sqrt{5/(R_{T2} - 1)} - 1)C_V\theta & R_{T2} > 21/16 \end{cases} \tag{34}$$

$${}_cA_H(x,y) = \sum_{i=1}^{2} |{}_cA_{Hi}(x,y)| \tag{35}$$

$${}_cA_V(x,y) = \sum_{i=1}^{2} |{}_cA_{Vi}(x,y)| \tag{36}$$

$$f_H(x,y) = m_k\ {}_cA_H(x,y), \quad f_V(x,y) = m_k\ {}_cA_V(x,y) \tag{37}$$

The proposed ridgeline *A-O-A′* (Figure 5) accelerations are compared with the mean NLRHA results in Figures 19 to 21. For comparison, results accounting only for the substructure T1 mode (${}_sA_{Heq1}$) with the corresponding roof amplification factors (F_{H1} and F_{V1}) are also shown and labelled 'T1' and for the substructure T2 mode (${}_sA_{Heq2}$) response obtained with the corresponding roof amplification factors (F_{H2} and F_{V2}) are also shown and labelled 'T2'.

The ductility ratios from the first mode T1 are large resulting in longer secant periods (Tables 9 and 11) and thereby smaller substructure accelerations from the first mode as depicted by the dotted T1 lines in Figures 19 to 21. The second mode accelerations achieve smaller ductility ratios (Tables 10 and 12) resulting in near-elastic peak substructure (${}_sA_{Heq2}$) response. Furthermore, the T2 mode exhibits shorter period ratios (R_{T2}) leading to larger vertical roof amplification factors and therefore, the higher mode contribution towards the overall vertical roof response is much larger than the first mode, even though the mass participation of the higher mode is small. Nevertheless, for $p = 10\%$, both N&K and Newmark methods present near identical responses for Model-B and Model-C (with T1 modes in the constant velocity region) and conservatively capture the mean DBE level NLRHA vertical response but underestimate the horizontal response (Figure 20(b) and (c)). For Model-A (with T1 mode in the constant acceleration region), the Newmark method presents the most conservative horizontal and vertical response among the proposed R-factor approaches. For DBE level response results using direct-R factor method, the accuracy is relatively low as it assumes much larger force reduction factors in both the modes and may not be realistic for multistorey structures with significant second mode contributions. For structures with higher post-yield stiffness like the $p = 25\%$ models, the peak substructure response is underestimated by the R-factor methods leading to unconservative overall peak roof responses (Figure 21) in all models. These errors increase as the level of the intensity increases from SLE to MCE with increasing ductility values. The more accurate Kasai method is therefore recommended for estimating responses of structures with higher post-yield stiffness ratios.

6-Storey analysis models

To further investigate the effects of substructure higher-modes, a 6-storey substructure with a height of 30m was also constructed as shown in the Figure 22. Commensurate with the geometry of the previous substructure models, the storey height for the 6-storey substructure is kept constant at 5m, each storey has a floor weight of 7kPa and the roof dead load is assumed to be 2kPa (Table 3). The gravity frame section sizes are also adopted from the 2-storey model given in Table 7. The BRBs were designed using the same design procedure (as discussed for 2-storey models using equation 17 and R=8) and a standard post-yield stiffness ratio p =2%, and the properties of the BRB links and design storey shears are given in Table 13. The combined analysis model (Model-B) was then constructed combining the roof model (Figure 5(b)) and the substructure model. To investigate the effect of post-yield stiffness, an additional substructure model with links modelled with a post-yield stiffness p =25% was created keeping the yield displacements the same. For brevity, only the Model-B is discussed in this paper for 6-storey models.

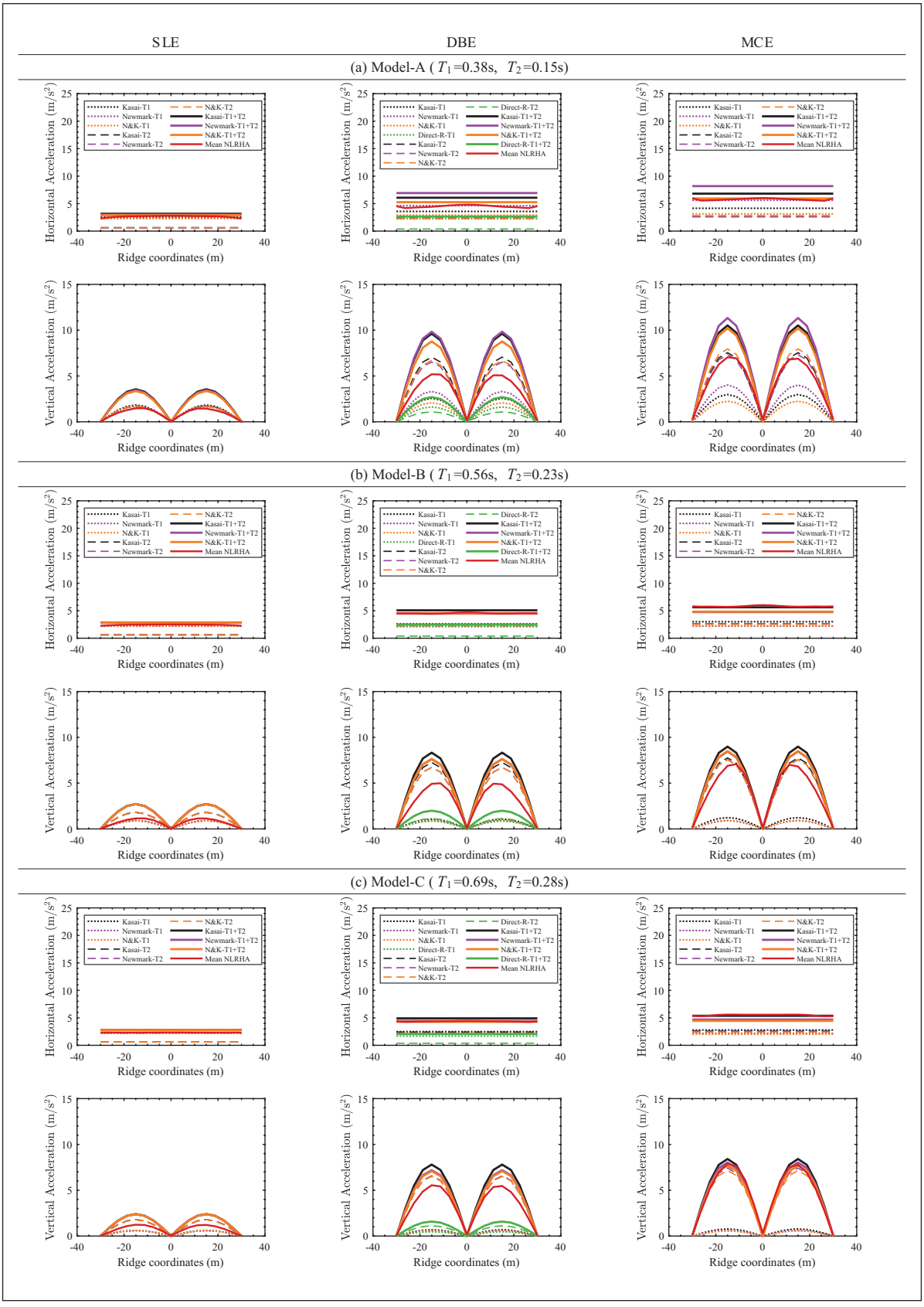

Figure 19. p = 2% 2-storey models: ridgeline accelerations: (a) Model-A (T_1 = 0.38 s, T_2 = 0.15 s), (b) Model-B (T_1 = 0.56s, T_2 = 0.23 s), and (c) Model-C (T_1 = 0.69s, T_2 = 0.28 s).

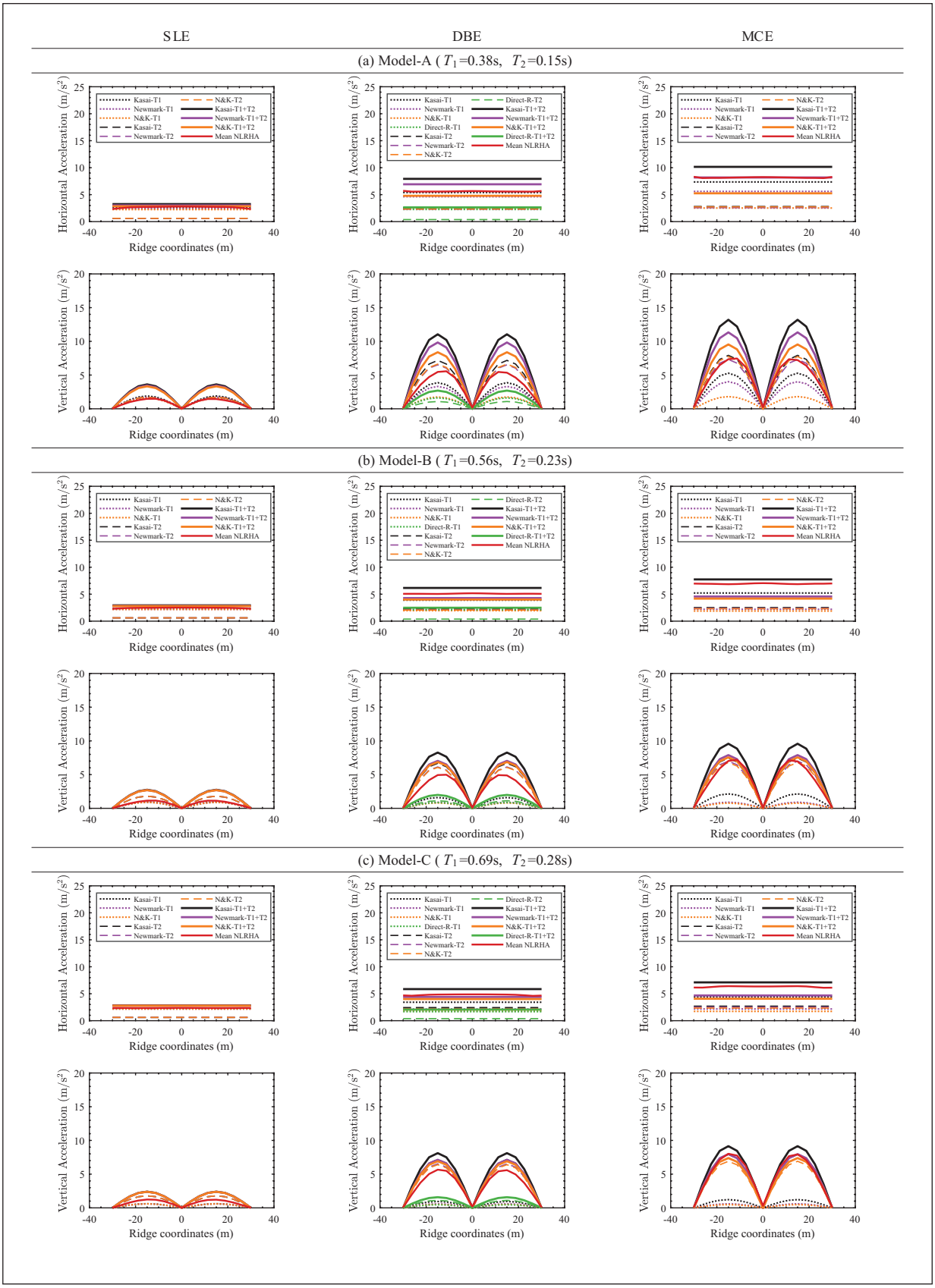

Figure 20. p = 10% 2-storey models: ridgeline accelerations: (a) Model-A (T_1 = 0.38 s, T_2 = 0.15 s), (b) Model-B (T_1 = 0.56 s, T_2 = 0.23 s), and (c) Model-C (T_1 = 0.69 s, T_2 = 0.28 s).

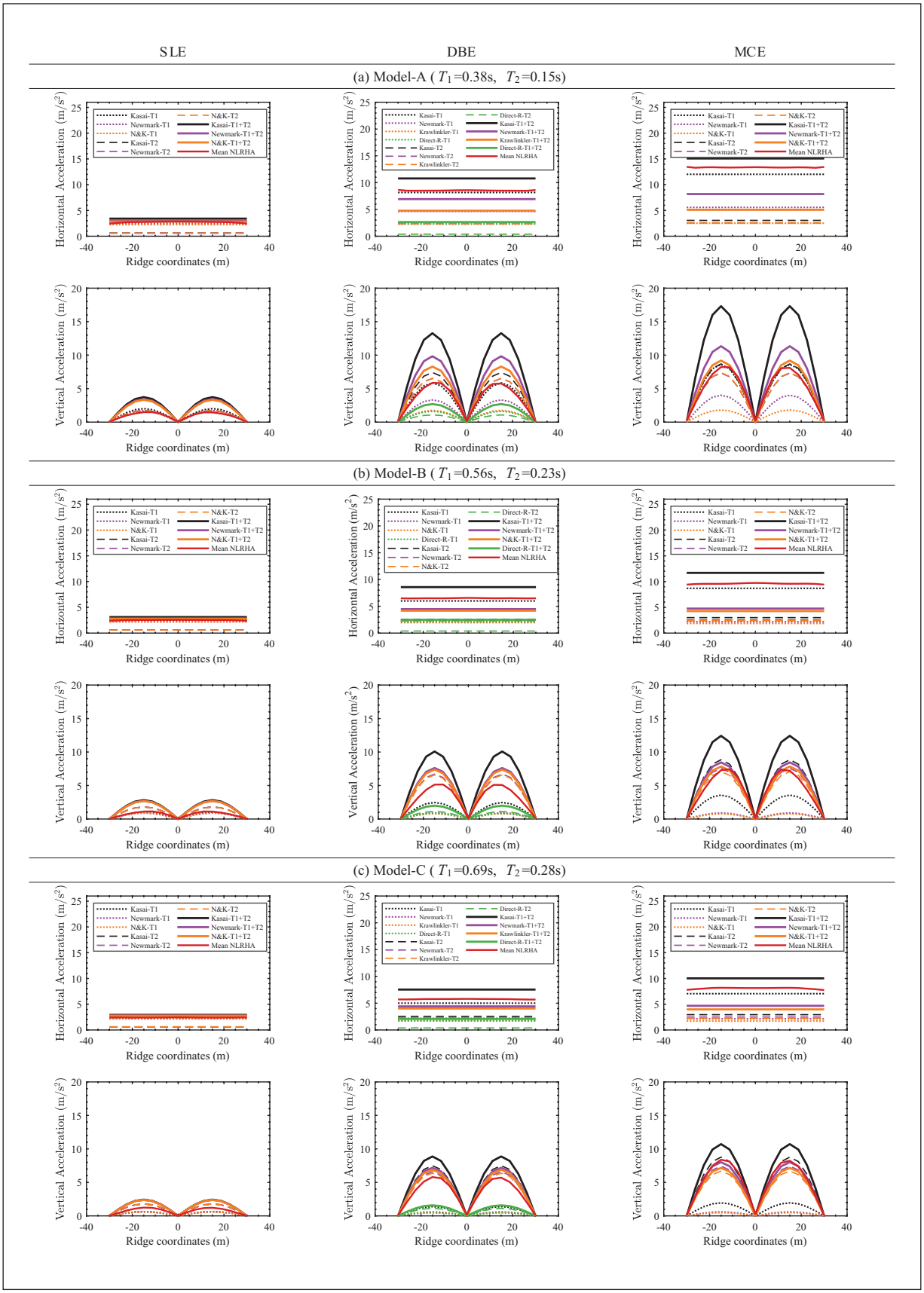

Figure 21. p = 25% 2-storey models: ridgeline accelerations: (a) Model-A (T_1 = 0.38 s, T_2 = 0.15 s), (b) Model-B (T_1 = 0.56 s, T_2 = 0.23 s), and (c) Model-C (T_1 = 0.69 s, T_2 = 0.28 s).

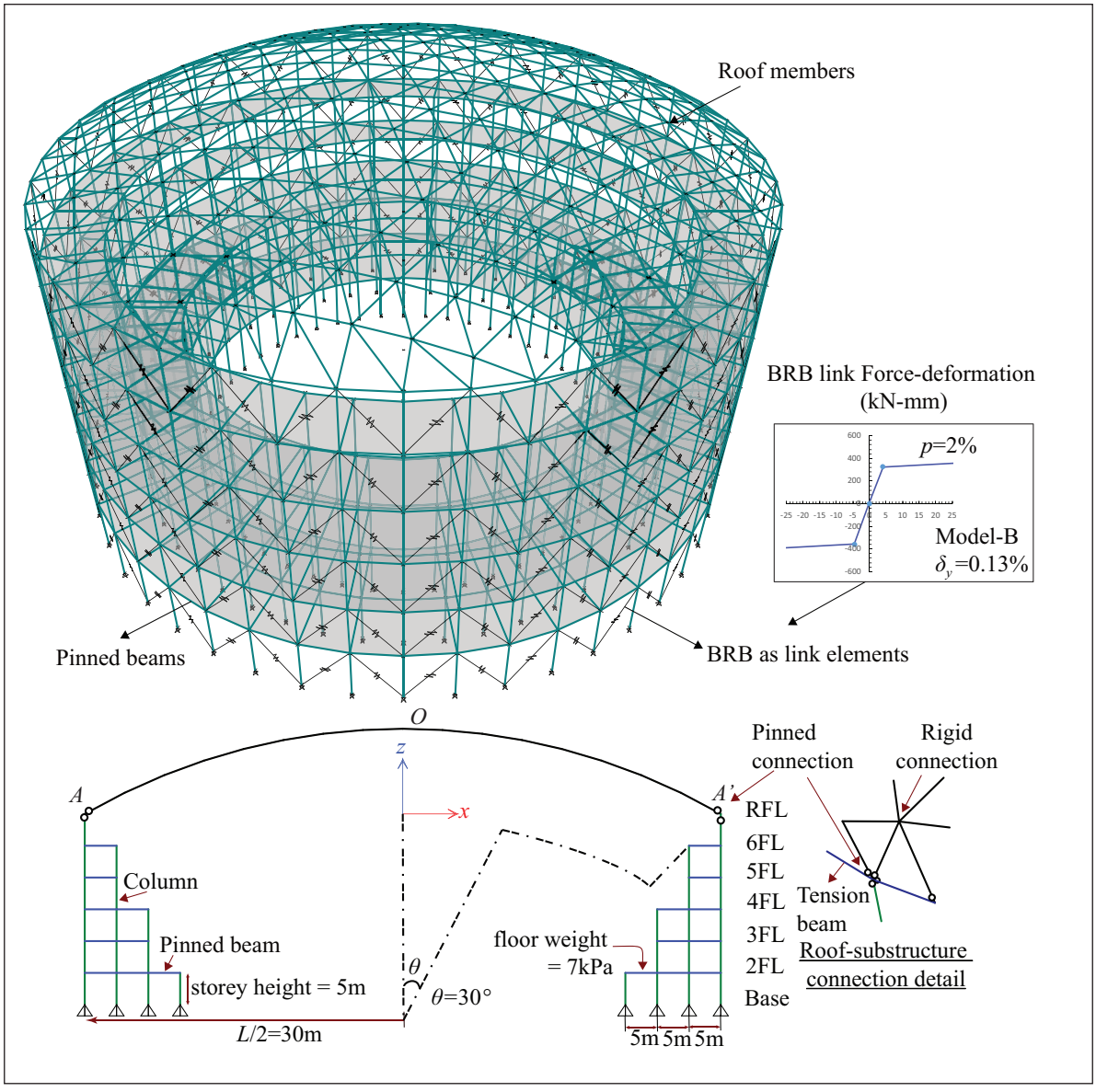

Figure 22. 6-storey Model-B (combined model): perspective and elevation view.

Table 13. 6-storey model: Equivalent lateral forces for proportioning BRBs (σ_y = 235 MPa).

Storey	h (m)	W_x (kN)	V_x (kN)	BRB V_x (kN)	BRB V_{ix} (kN)	BRB P_i (kN)	δ_y (mm)	BRB K_{eqi} (kN/m)	A_c (mm^2)
Model-B (T_1 = 0.93s, T_2 = 0.39s)									
RFL	30	6064	1483	1483	43	75	4.12	18,343	321
6FL	25	6032	2713	2713	77	138	4.12	33,550	588
5FL	20	6032	3696	3696	106	188	4.12	45,715	801
4FL	15	10968	5038	5038	144	256	4.12	62,305	1091
3FL	10	10968	5932	5932	169	302	4.12	73,364	1285
2FL	5	10968	6379	6379	182	325	4.12	78,894	1382

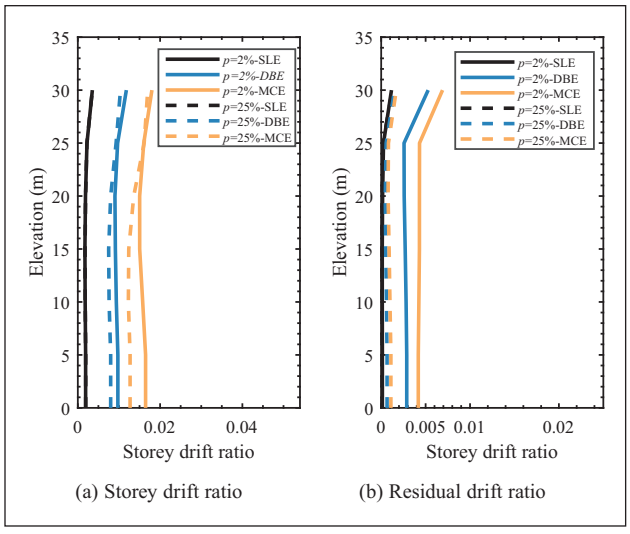

Figure 23. 6-storey Model-B: Mean of peak storey drift ratios of substructure: (a) storey drift ratio and (b) Residual drift ratio.

6-storey models: Inter-storey drifts

The mean peak inter-storey drifts and mean residual inter-storey drifts for the substructure of the combined models (Model-B) are given in Figure 23. ASCE-7[1] prescribes an allowable storey drift of 2.0% for DBE level. The obtained mean storey drifts are quite uniform along the substructure height and are within the permissible ASCE limits for all the models with post-yield stiffness. Typical values of mean residual drift are about 0.3% for p=2% models under the DBE level. These values increase to 0.4% under the MCE level and are within the 0.5% limit for immediate occupancy criteria for most stories except the roof floor. While increasing the post-yield stiffness to p=25% reduces the peak inter-storey drifts, the improvement in residual drifts is much more significant with typical residual drifts for all the three levels within 0.2%.

6-storey models: Peak substructure acceleration

The first substructure mode T1 (fundamental translational mode) has a period of 0.93 s and a mass participation (Γ_1) of 77% and the second translational mode T2 has a period of 0.39 s and contributes to a mass participation (Γ_2) of 15%. The periods are longer than those of the 2-storey models resulting in longer period ratios. These longer period ratios imply that the roof-substructure interaction is weaker and corresponds to smaller vertical amplification factors which have an inverse relationship with the period ratios in this range. The mass participation of second mode is larger if compared to the 2-storey substructure models, leading to higher contribution of the T2 mode to the peak substructure response.

For each of the models, modal pushover analyses was conducted to obtain the first and second modal pushover curves and initial base shear to roof displacement stiffness (K_{1i}) was obtained as shown in Figure 24. For $p = 2\%$ model, the first mode pushover curve has a post-yield stiffness of 2% and the second mode pushover curve was found to have a higher post-yield stiffness of 14% as the BRBs of all the storeys do not yield at the same time and many of the braces remain elastic when the substructure is pushed using a force distribution based on the second mode shape. Similarly, for the $p = 25\%$ model, the first mode pushover curve has a post-yield stiffness of 25% and the second mode pushover curve was found to have a post-yield stiffness ratio of 36%.

As for the 2-storey and single-storey models, the peak response of each model was computed for three levels of earthquake intensity – SLE, DBE and MCE. The reduction in acceleration (R_{ai}) and achieved damping parameters for each substructure mode from the Kasai method are given in Tables 14 to 17. For the DBE level, as both the seismic demand and reduction factors are large, the roof displacement ductility factors obtained from the first mode μ_1 were about 6. The second mode had a significant contribution to damping as well as can be seen from the higher h_{eq2} values and lower D_{h2} values in Tables 15 and 17 if compared to the 2-storey models in Tables 10 and 12. The shift in periods and reduction in acceleration was thus larger than those observed for the second mode in 2-storey models.

6-storey models: Peak roof response

After obtaining the peak substructure response, the peak roof accelerations for the combined models were calculated for each of the modes from the inelastic response ${}_sA_{Heqi}$ and the corresponding first and second mode amplification factors in equations (23)–(28). The peak roof accelerations for the combined models listed in Tables 14 to 17 were calculated using the first and second mode amplification factors in equations (23)–(28). The proposed envelope of ridgeline *A-O-A′* (Figure 22) accelerations are compared with the mean NLRHA results in Figures 25 and 26. The second mode achieves smaller ductility ratios (Tables 15 and 17) and the reduction in acceleration is lesser if compared to the T1 mode response. Therefore, in large ductility regimes for the DBE and MCE levels, ${}_sA_{Heq2}$ (T2 dashed lines) is higher than ${}_sA_{Heq1}$ (T1 dotted lines). Furthermore, the T2 mode exhibits relatively shorter period ratios ($R_{T2} < R_{T1}$) leading to larger vertical roof amplification factors ($F_{V2} > F_{V1}$) and therefore, the higher mode contribution towards the overall vertical roof response is much larger than the first mode, even though the mass participation of the higher mode is small. For $p = 2\%$ DBE level response results

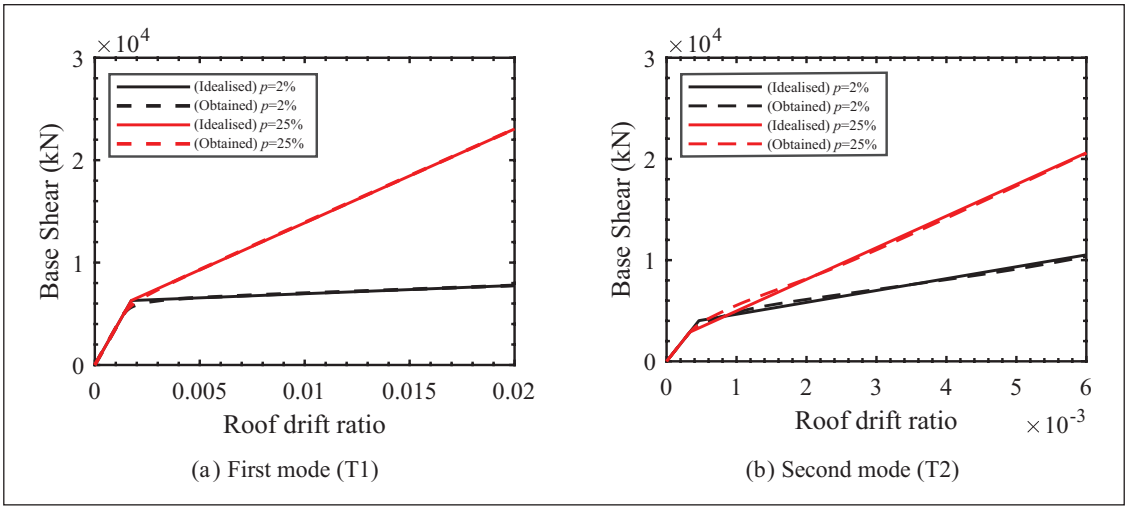

Figure 24. 6-storey Model-B: modal pushover curves and idealisation of structural response: (a) first mode (T1) and (b) second mode (T2).

Table 14. 6-storey $p = 2\%$ models: peak substructure first-mode (T1) parameters.

	h_{eq1}	K_{eq1}/K_1	D_h	R_d	R_a	μ_{t1}	T_1	T_{eq1}	T_R
Model-B-SLE	0.06	0.87	0.97	1.04	0.91	1.11	0.94	1.00	0.23
Model-B-DBE	0.37	0.18	0.47	1.10	0.20	5.53	0.94	2.19	0.23
Model-B-MCE	0.43	0.11	0.44	1.30	0.15	8.30	0.94	2.78	0.23

Table 15. 6-storey $p = 2\%$ models: peak substructure second-mode (T2) parameters.

	h_{eq2}	K_{eq2}/K_2	D_h	R_d	R_a	μ_{t2}	T_2	T_{eq2}	T_R
Model-B-SLE	0.05	1.00	1.00	1.00	1.00	1.00	0.39	0.39	0.23
Model-B-DBE	0.23	0.43	0.58	1.08	0.46	2.96	0.39	0.60	0.23
Model-B-MCE	0.31	0.33	0.51	1.10	0.36	4.44	0.39	0.69	0.23

Table 16. 6-storey $p = 25\%$ models: peak substructure first-mode (T1) parameters.

	h_{eq1}	K_{eq1}/K_1	D_h	R_d	R_a	μ_{t1}	T_1	T_{eq1}	T_R
Model-B-SLE	0.05	0.91	0.98	1.03	0.94	1.11	0.94	0.98	0.23
Model-B-DBE	0.20	0.39	0.61	0.98	0.38	5.53	0.94	1.49	0.23
Model-B-MCE	0.20	0.34	0.61	1.04	0.35	8.29	0.94	1.60	0.23

Table 17. 6-storey $p = 25\%$ models: peak substructure second-mode (T2) parameters.

	h_{eq2}	K_{eq2}/K_2	D_h	R_d	R_a	μ_{t2}	T_2	T_{eq2}	T_R
Model-B-SLE	0.05	1.00	1.00	1.00	1.00	1.00	0.39	0.39	0.23
Model-B-DBE	0.19	0.51	0.63	1.05	0.54	4.13	0.39	0.55	0.23
Model-B-MCE	0.20	0.46	0.61	1.08	0.50	6.20	0.39	0.58	0.23

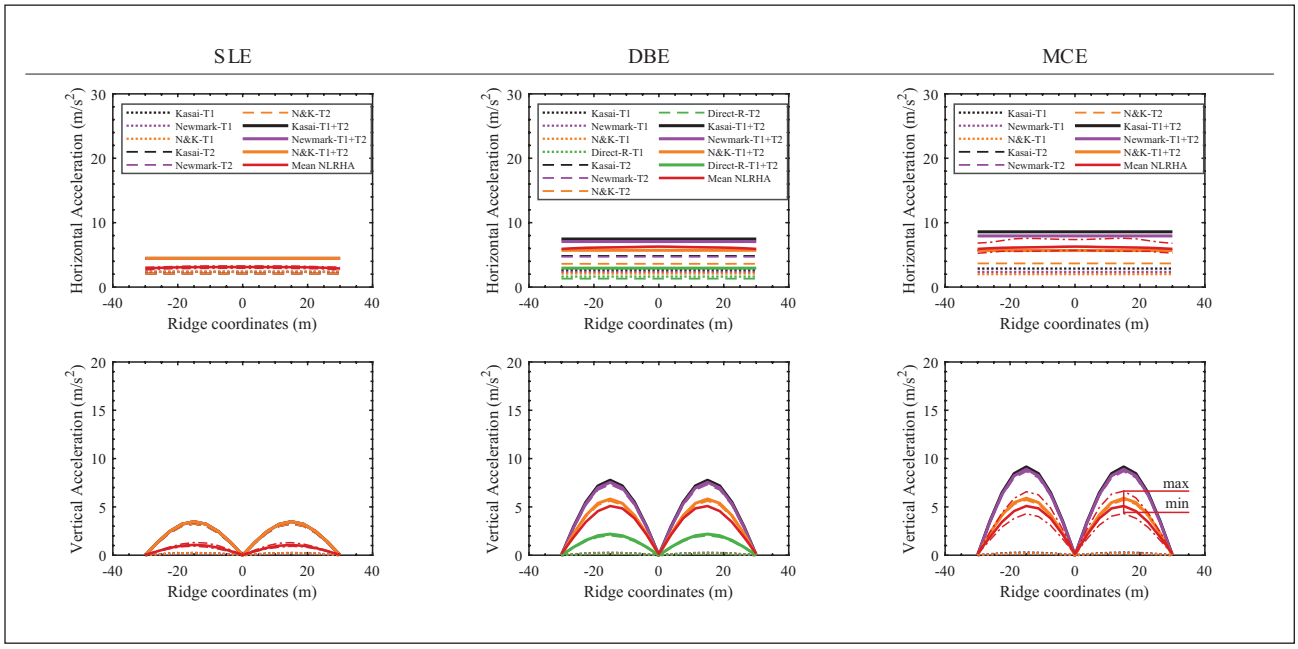

Figure 25. 6-storey (Model-B: T_1 = 0.94 s, T_2 = 0.39 s) p = 2%: ridgeline accelerations.

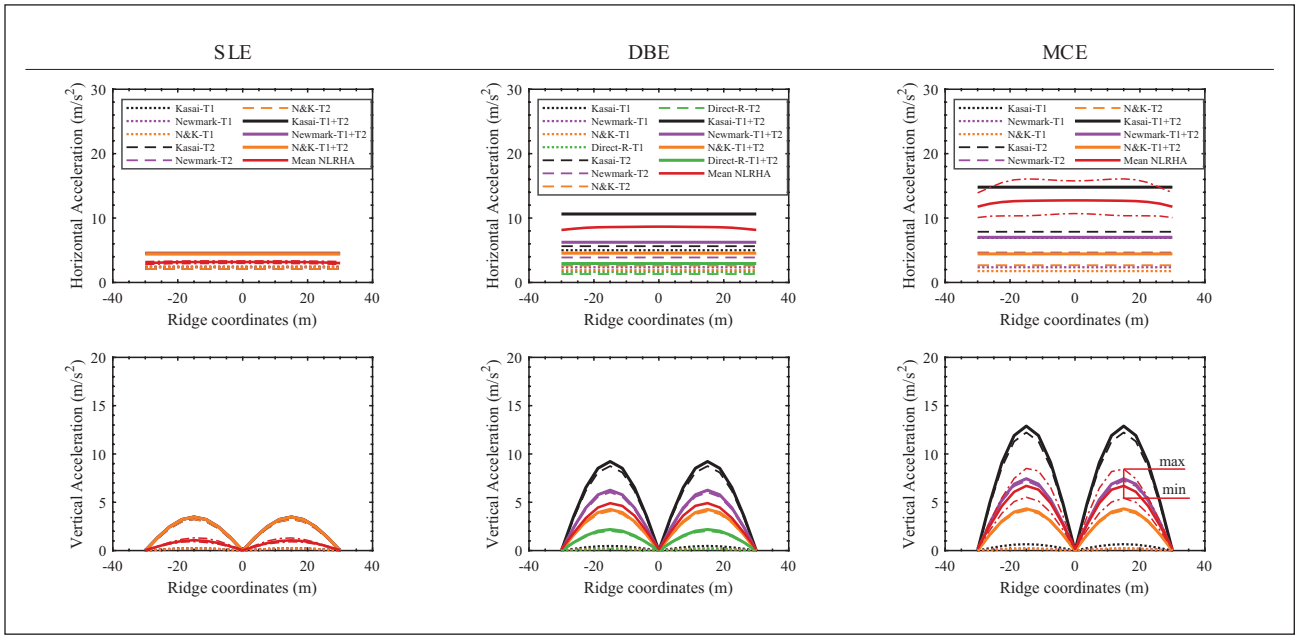

Figure 26. 6-storey (Model-B: T_1 =0.94s, T_2 =0.39s), p = 25% : ridgeline accelerations.

using direct-R factor method, the accuracy is relatively low as it assumes much larger force reduction factors than actually achieved in both the modes (severely underestimating the second mode response) and may not be realistic for multistorey structures with significant second mode contributions. However, the response from Newmark's method (T1 + T2 response) is nearly equal to the Kasai method (T1 + T2 response) in Figure 25, conservatively capturing the mean NLRHA response. For the Newmark method, the ${}_sA_{Heq1}$ was computed following the equal displacement rule and ${}_sA_{Heq2}$ using the equal energy rule as the two substructure modes lie on different regions of the spectrum. This confirms the applicability of Newmark method for multistorey substructures with elastoplastic first mode response and considerable post-yield stiffness in the second mode.

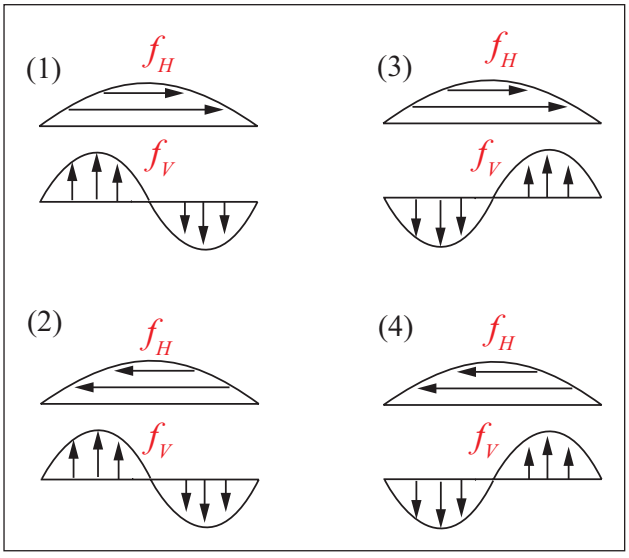

Figure 27. Static load patterns.

As observed in the previous 2-storey models (Figures 17 and 18), for structures with higher post-yield stiffness like the $p = 25\%$ models, the peak substructure response is underestimated by the R-factor methods leading to unconservative overall peak roof responses (Figure 26). These errors increase as the level of the intensity increases from SLE to MCE with increasing ductility values. Nevertheless, the Newmark method provided a conservative estimate of the vertical response even for $p = 25\%$ models as the proposed vertical amplification factors are conservative enough to compensate for the underestimation of the substructure response. To summarise, the most conservative Kasai method is recommended for estimating responses of structures with higher post-yield stiffness ratios.

Equivalent static loads

The proposed peak roof accelerations were then used to compute the corresponding equivalent static loads using equation (37). Static analyses were performed by applying the obtained vertical and horizontal loads simultaneously to the roof nodes in each of the patterns (corresponding to the roof's dominant anti-symmetric mode shape O1 expressed by equations (27) and (28)) as shown in Figure 27.[13] The maximum response (axial force and bending moment) in each member from the four static load cases may be considered as the preliminary seismic demand.

The detailed results for the 2-storey $p = 2\%$ and $p = 25\%$ models are compared with the mean NLRHA response in Figures 28 and 29. The proposed fit lines are also shown using dashed lines. The axial forces from the R-factor approaches are close to the NLRHA response except for the direct-R method. Furthermore, the R-factor methods' and the Kasai method's member responses are nearly equal for models with $p = 2\%$. For $p < 10\%$, all the estimation methods present near identical responses for Model-B and Model-C (with T1 modes in the constant velocity region) accurately capturing the mean NLRHA response. For Model-A (with T1 mode in the constant acceleration region), the Newmark method followed by the Kasai method present the most conservative response among the investigated estimation methods. The errors in the R-factor methods are more evident in the models with higher post-yield stiffness (Figure 29) where the Kasai method (shown in black markers) exhibits much more conservative DBE and MCE level axial forces and bending moments when compared to the NLRHA method. As discussed in the previous sections of peak roof responses, this is due to the underlying assumptions of R-factor approaches which were proposed considering idealised elastoplastic (or low post-yield stiffness) backbone behaviour and thus are recommended for models with relatively low post-yield stiffness.

The member responses of the 6-storey models are also compared in detail in Figures 30 and 31. While the second mode possesses higher post-yield stiffness in the 6-storey cases, similar to the 2-storey models' responses, the accuracy of the Newmark method and the Kasai method remained nearly equal for models with $p = 2\%$. As observed for the peak ridge accelerations, the differences in proposed member forces are more evident in the models with higher post-yield stiffness where the Kasai method exhibits a more conservative response with the errors in the R-factor method estimates larger in the higher ductility ranges (the DBE and MCE level). As the equivalent static load results from the proposed RSA and amplification factor approach provide an enveloped response, the obtained axial forces and bending moments do not necessarily correspond to the critical combination of the forces and moments obtained from the response-history analyses.[5,7] Therefore, it is recommended to use the proposed equivalent static load procedure in the preliminary design stages as a baseline method for initial sizing and approximate estimation of the member forces. For the final design member check, it is recommended to use the more rigorous NLRHA method.

Conclusions

This paper investigated the applicability of the ductility-based reduction factors to estimate the peak substructure response (R-factor approaches) using RSA which forms the basis for the equivalent static forces of the dome. The response of simpler single-storey substructures and the higher mode effects of multistorey substructures were studied and the results from the proposed estimation methods were verified using nonlinear response history

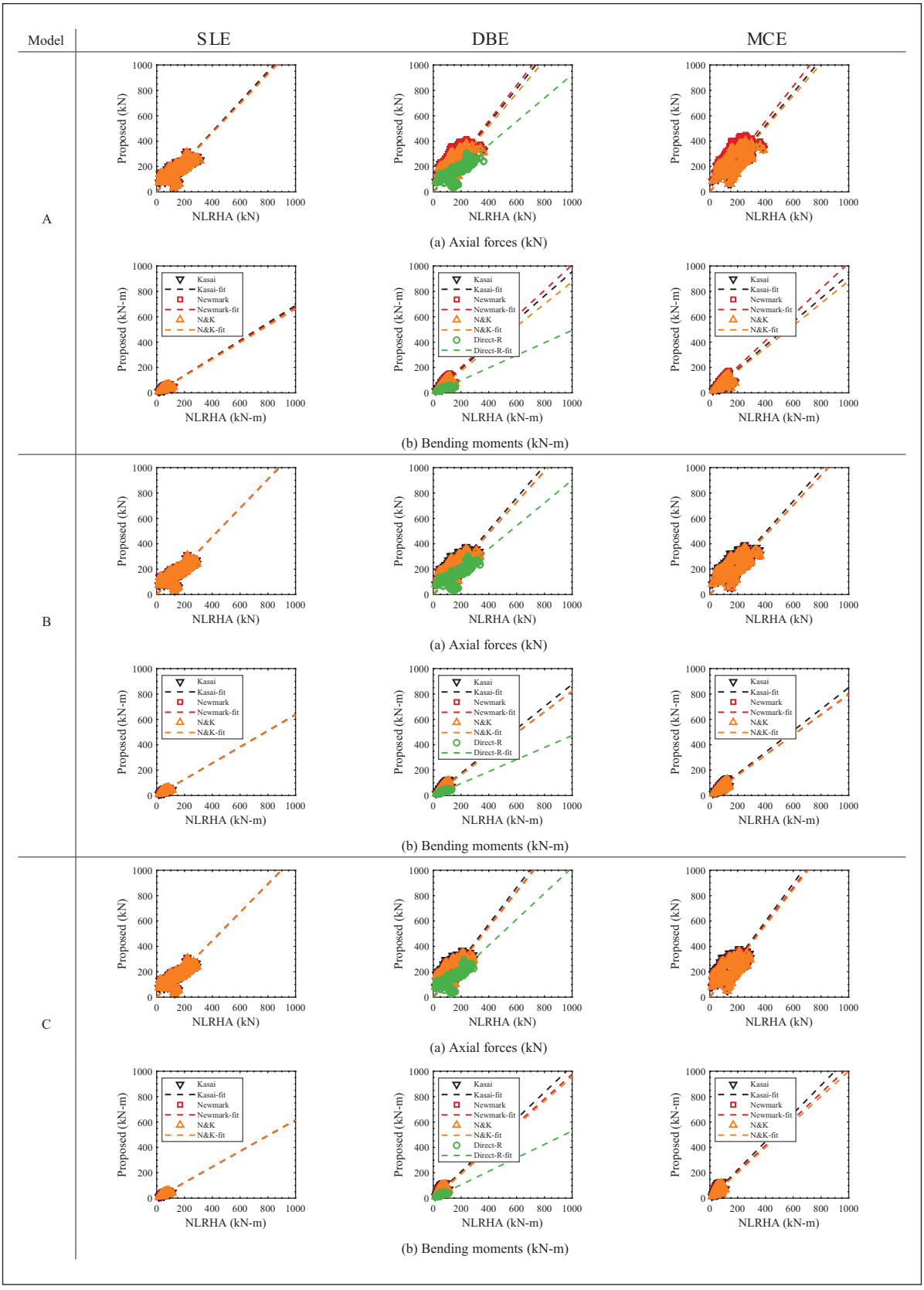

Figure 28. 2-storey $p = 2\%$ models: Comparison of member axial forces and bending moments: (a) axial forces (kN) and (b) bending moments (kN m).

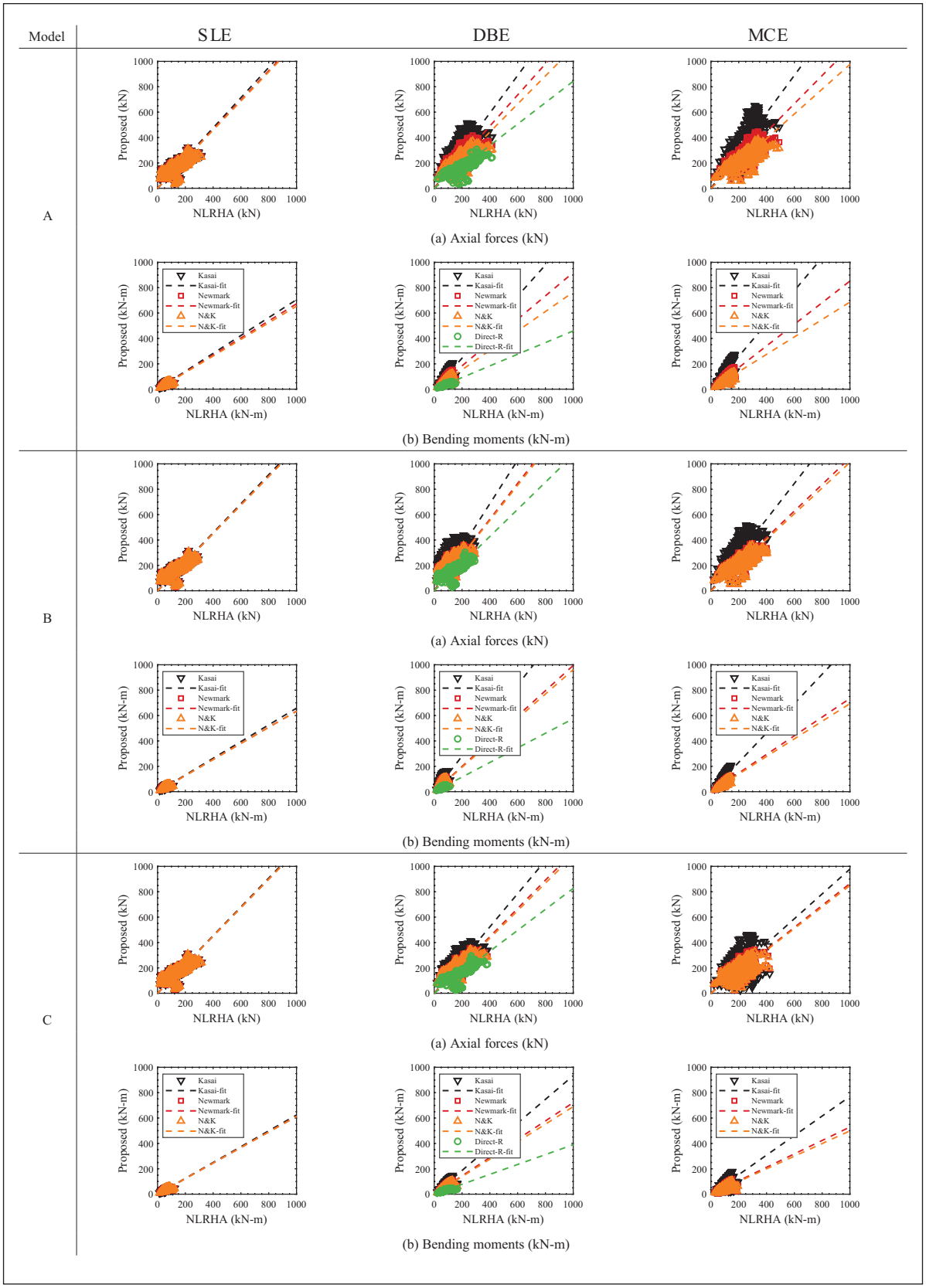

Figure 29. 2-storey $p = 25\%$ models: comparison of member axial forces and bending moments: (a) axial forces (kN) and (b) bending moments (kN m).

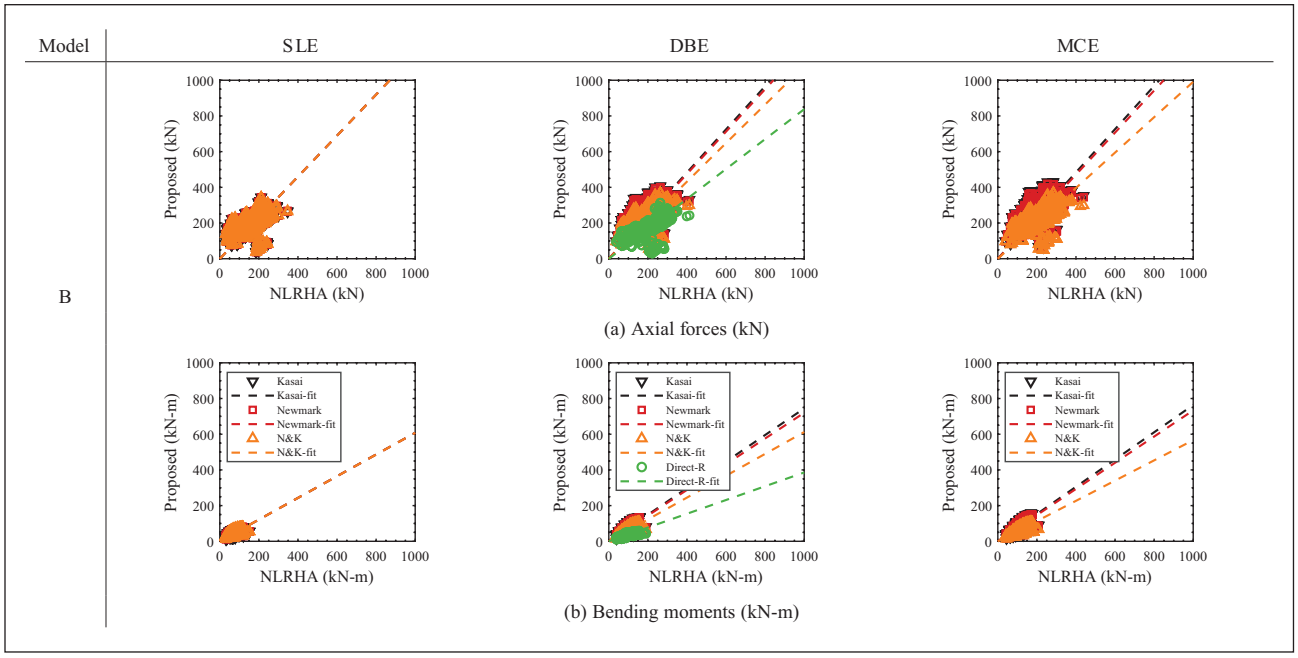

Figure 30. 6-storey $p = 2\%$ models: Comparison of member axial forces and bending moments: (a) axial forces (kN) and (b) bending moments (kN m).

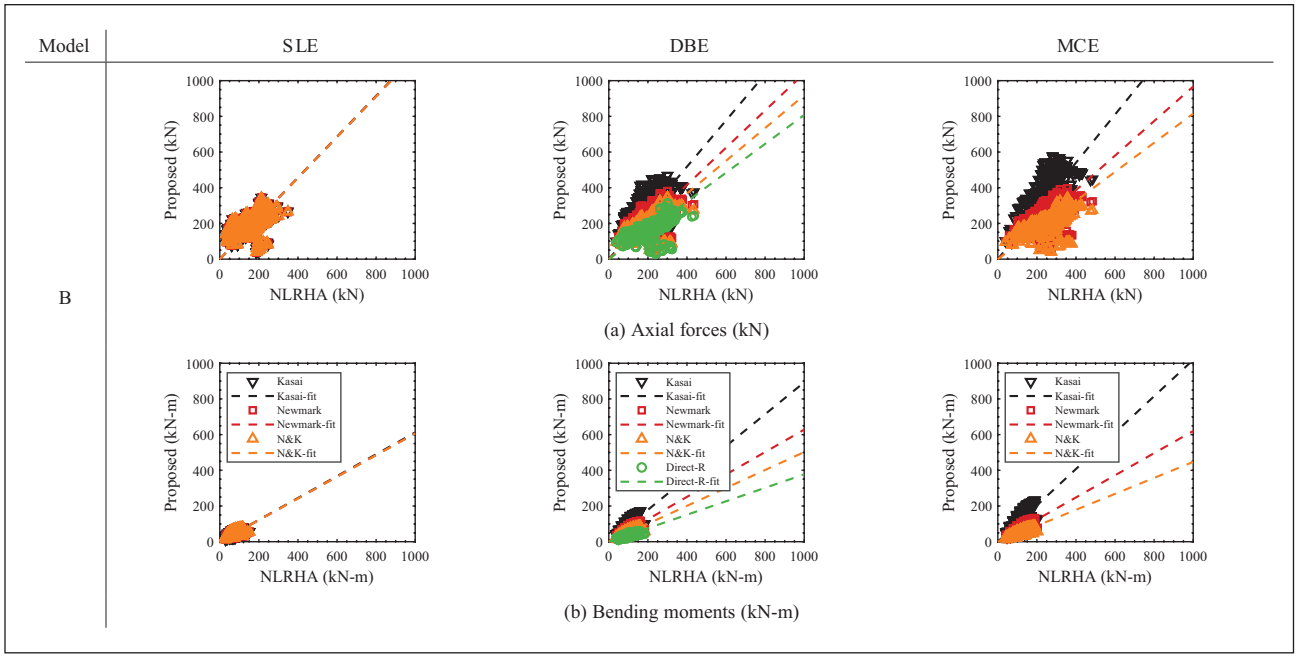

Figure 31. 6-storey $p = 25\%$ models: Comparison of member axial forces and bending moments: (a) axial forces (kN) and (b) bending moments (kN m).

analyses (NLRHA). The following conclusions were drawn from this investigation:

1. The RSA based amplification factor approach proposed for elastic structures was extended for practical yielding BRBF substructures designed using an *R*-factor of 8 and varying the post-yield stiffness. It was observed that the peak inelastic roof response was highly influenced by the post-yield stiffness (p) of the substructure, and so

adopting the same *R*-factor (=8) for obtaining the inelastic force demands (as in the 'direct-R' method) severely underestimated the peak roof responses for models with $p > 2\%$.

2. Kasai's equivalent linearisation method estimated the substructure response with accuracies very similar to the NLRHA for all the studied models. This method used in combination with the proposed amplification factor approach is an efficient alternative to the NLRHA method to estimate a conservative envelope of the peak accelerations and the equivalent static loads for the preliminary design of the dome.
3. For single-storey and first-mode dominated structures, both the R-factor methods – 'Newmark' and 'Nassar & Krawlinkler' apply simple ductility reduction factor formulations to estimate the peak substructure responses and the accuracies are comparable to those from the NLRHA for structures with low post-yield stiffness ratios ($p <= 2\%$). The Newmark method formulated based on the equal energy rule was found to have the best accuracy among the R-factor approaches for short-period structures with fundamental periods in the constant acceleration region of the design acceleration spectrum.
4. The accuracies of the R-factor methods in estimating the peak substructure response was low for single and 2-storey structures with high post-yield stiffness ratios ($p = 25\%$) due to the underlying assumptions behind the formulations. Therefore, for structures with high post-yield stiffness ratios ($p >= 2\%$) typically found in countries like Japan with moment connections, it is recommended to adopt the more accurate Kasai method in combination with the amplification factors to obtain the peak envelope roof response. These may then be used to obtain the equivalent static loads on the roof for preliminary member sizing.
5. While multistorey structures exhibit significant higher mode response, for substructures with low (first-mode) post-yield stiffness ratios, Newmark's method in combination with the first and second mode amplification factors provides a conservative roof response with accuracies nearly equal to those of the iterative Kasai method. Therefore, for all structures with low post-yield stiffness ratios ($p < 10\%$), it is recommended to adopt the simpler Newmark method in combination with the amplification factors to obtain the envelope of the peak roof response.

Declaration of conflicting interests

The author(s) declared no potential conflicts of interest with respect to the research, authorship, and/or publication of this article.

Funding

The author(s) received no financial support for the research, authorship, and/or publication of this article.

ORCID iD

Deepshikha Nair https://orcid.org/0000-0003-3223-3303

References

1. ASCE Standard–ASCE/SEI 7–16. *Minimum design loads for buildings and other structures*. American Society of Civil Engineers, 2016.
2. NZS 1170.5:2004. *Structural design actions part 5: earthquake actions – New Zealand*. Wellington: Standards New Zealand, 2004.
3. British Standard–Eurocode 8. *Design of structures for earthquake resistance: Part 1*. British Standards, 2005.
4. The Building Center of Japan. *The building standard law of Japan on CD-ROM*. The Building Center of Japan, 2016.
5. International Association for Shell and Spatial Structures. *Guide to earthquake response evaluation of metal roof spatial structures, working group 8*. The International association for Shell and Spatial structures, 2019.
6. Nakazawa S, Kato S, Takeuchi T, et al. State-of-the-art of seismic response evaluation methods for metal roof spatial structures. *J Int Assoc Shell Spatial Struct* 2012; 53:117–130.
7. Takeuchi T, Ogawa T and Kumagai T. Seismic response evaluation of lattice shell roofs using amplification factors. *J Int Assoc Shell Spatial Struct* 2007; 48:197–210.
8. Kato S, Nakazawa S and Saito K. Two-mode based estimation of equivalent seismic loads and static estimation of dynamic response of reticular domes supported by ductile substructures. *J Int Assoc Shell Spatial Struct* 2006; 47:35–52.
9. Kawaguchi M and Kato S. Metal space structures. *J Int Assoc Shell Spatial Struct* 2001; 42:21–26.
10. Kato S, Ueki T and Mukaiyama Y. Study of dynamic collapse of single layer reticular domes subjected to earthquake motion and the estimation of statically equivalent seismic forces. *Int J Space Struct* 1997; 12(3–4): 191–203.
11. Yamada S. Vibration behaviour of single-layer latticed cylindrical roofs. *Int J Space Struct* 1997; 12(3–4): 181–190.
12. Takeuchi T, Kumagai T, Okayama S, et al. Seismic response evaluation of low-to-high rise lattice domes. In: *Proceedings of APCS* 2009, Nagoya, Japan, 2009, pp.71–72.
13. Nair D, Terazawa Y, Sitler B, et al. Seismic response of long-span domes supported by multi-storey substructures. *J Int Assoc Shell Spatial Struct* 2020; 61:140–157.
14. Takeuchi T, Ogawa T, Nakagawa M, et al. Response evaluation of medium-span lattice domes with substructures using response spectrum analysis. In: *IASS2004 symposium*, Montpellier.
15. Takeuchi T, Kumagai T, Shirabe H, et al. Seismic response evaluation of lattice roofs supported by multistory substructures. In: *Shell and spatial structures: structural architecture – towards the future looking to the past. IASS symposium*, Venice, Italy, p.362.
16. Nair D, Ichihashi K, Terazawa Y, et al. Higher mode effects of multistorey substructures on the seismic response of

double-layered steel gridshell domes. *Eng Struct* 2021; 243:112677.
17. Takeuchi T, Xue SD, Nakazawa S, et al. Recent applications of response control techniques to metal spatial structures. *J Int Assoc Shell Spatial Struct* 2012; 53(2): 99–110.
18. Kumagai T, Takeuchi T, Ogawa T, et al. Seismic response evaluation of latticed domes with elasto-plastic substructures using amplification factors. In: *Proceedings of IASS*, Bucharest, Romania, 2005, pp.383–390.
19. Kato S and Nakazawa S. Seismic design method to reduce the responses of single layer reticular domes by means of yielding of substructure under severe earthquake motions. In: Proceedings of IASS, Nagoya, Japan, 2001, p.TP077.
20. Kasai K, Ito H and Watanabe A. Peak response prediction rule for a SDOF elasto-plastic system based on equivalent linearization technique. *J Struct Constr Eng* 2003; 68(571): 53–62.
21. Kasai K and Ito H. JSSI manual for building passive control technology. Part. 8 Peak response evaluation and design for elastoplastically damped system. In 13th world conference on earthquake engineering, Vancouver, BC, Canada, paper no. 5060.
22. Kaneda K. Endeavors to control the vibration on long span structure. In: *Proceedings of international symposium on theory, design and realization of shell and spatial structures*, Nagoya, 2001.
23. Hosozawa O and Mizutani T. Structural design of Simokita dome. In: Proceedings of IASS, Bucharest, 2005, p.707.
24. Takeuchi T, Ogawa T, Suzuki T, et al. A basic study on damage-controlled design concept for truss frame structures. *J Struct Constr Eng* 2005; 51:31–37.
25. Takeuchi T, Tsutsumi T, Ogawa T, et al. Seismic retrofit of steel-structure school gymnasia with energy dissipation braces. In: Proceedings of IASS, Shanghai, 2010.
26. Fahnestock LA, Sause R and Ricles JM. Seismic response and performance of buckling-restrained braced frames. *J Struct Eng* 2007; 133(9): 1195–1204.
27. Güner T and Topkaya C. Performance comparison of BRBFs designed using different response modification factors. *Eng Struct* 2020; 225:111281.
28. Uang C. Establishing R (or R_w) and C_d factors for building seismic provisions. *J Struct Eng* 1991; 117(1): 19–28.
29. Riddell R, Hidalgo P and Cruz E. Response modification factors for earthquake resistant design of short period buildings. *Earthq Spectra* 1989; 5(3): 571–590.
30. Riddell R. Inelastic response spectrum: early history. *Earthq Eng Struct Dyn* 2008; 37(8): 1175–1183.
31. Nassar A, Osteraas J and Krawinkler H. Seismic design based on strength and ductility demands. In: *10th world conference on earthquake engineering*, Madrid, Spain, vol. 10, pp.5861–5866.
32. Lee LH, Han SW and Oh YH. Determination of ductility factor considering different hysteretic models. *Earthq Eng Struct Dyn* 1999; 28(9): 957–977.
33. King M, Whitby W and Hanshaw G. Design of the Singapore sports hub roof with high strength niobium steel. In: *IABSE symposium report*, Kolkata, India, vol. 101, pp.1–8. International Association for Bridge and Structural Engineering.
34. Takeuchi T and Wada A. *Buckling-restrained braces and applications*. Japan Society of Seismic Isolation, 2017.
35. Computers and Structures. *Analysis reference manual for SAP2000, ETABS, SAFE and CSIBridge*. Berkeley, CA: Computers and Structures, Inc, 2015.
36. Wilson EL. Three-dimensional static and dynamic analysis of structures. *Comput Struct* 2002 Fourth edition: 37–47.
37. American Institute of Steel Construction. *Specification for structural steel buildings (ANSI/AISC 360–16)*. American Institute of Steel Construction, 2016.
38. Rutten D. Grasshopper3d, 2015.
39. Pacific Earthquake Engineering Research Center and PEER Ground Motion Database. NGA West2, https://ngawest2.berkeley.edu/ (2020, accessed 13 March 2021).
40. Chandler AM and Duan XN. Performance of asymmetric code-designed buildings for serviceability and ultimate limit states. *Earthq Eng Struct Dyn* 1997; 26(7): 717–735.
41. Erochko J, Christopoulos C, Tremblay R, et al. Residual drift response of SMRFs and BRB frames in steel buildings designed according to ASCE 7-05. *J Struct Eng* 2011; 137(5): 589–599.